Renewable and Sustainable Energy Reviews 23 (2013) 60–79

Contents lists available at SciVerse ScienceDirect

Renewable and Sustainable Energy Reviews

journal homepage: www.elsevier.com/locate/rser

Heat transfer and fluid flow analysis of solar air heater: A review of CFD approach

Anil Singh Yadav*, J.L. Bhagoria

Mechanical Engineering Department, Maulana Azad National Institute of Technology, Bhopal, MP 462051, India

A R T I C L E I N F O

Article history:
Received 17 August 2012
Received in revised form
13 February 2013
Accepted 18 February 2013
Available online 21 March 2013

Keywords:
Solar energy
Solar air heater
CFD
Fluid flow
Pressure drop

A B S T R A C T

The objective of this article is to present a detailed review of the literature that deals with the application of CFD in the design of solar air heater. Solar air heater is one of the basic equipment through which solar energy is converted into thermal energy. CFD is a simulation tool which uses powerful computer and applied mathematics, to model fluid flow situations for the prediction of heat, mass and momentum transfer and optimal design in various heat transfer and fluid flow processes. The quality of the solutions obtained from CFD simulations are largely within the acceptable range proving that CFD is an effective tool for predicting the behavior and performance of a solar air heater. One of the great challenges in the design of a solar air heater using CFD approach is the selection of appropriate turbulence model. The decision about a suitable turbulence model chosen in a CFD computation is not easy. In this article a CFD investigation is also carried out to select best turbulence model for the design of a solar air heater. A modern CFD code ANSYS FLUENT v12.1 is used to simulate fluid flow through a conventional solar air heater. A two-dimensional flow is assumed. The influences of the five different turbulence models on the quality of the obtained results are tested. It appears from the performed calculations that the Renormalization-group k–ε model yields the best results for two-dimensional flow through conventional solar air heaters.

Contents

* Corresponding author. Tel.: +91 922 9220126.
E-mail address: anilsinghyadav@gmail.com (A.S. Yadav).

1364-0321/$ - see front matter © 2013 Elsevier Ltd. All rights reserved.
http://dx.doi.org/10.1016/j.rser.2013.02.035

Nomenclature

A_c	surface area of absorber plate (m^2)
C_p	specific heat of air (J/kg/K)
D	equivalent or hydraulic diameter of duct (m)
e	rib height (m)
h	heat transfer coefficient ($W/m^2/K$)
H	depth of duct (m)
I	turbulence intensity/intensity of solar radiation (W/m^2)
k	thermal conductivity of air (W/m/K)
L	length of duct (m)
L_1	inlet length of duct (m)
L_2	test length of duct (m)
L_3	outlet length of duct (m)
m	mass flow rate (kg/s)
ΔP	pressure drop (Pa)
P	pitch (m)
q_u	useful heat flux (W/m^2)
Q_u	useful heat gain (W)
Q_L	heat loss from collector (W)
Q_t	heat loss from top of collector (W)
T_o	fluid outlet temperature (K)
T_i	fluid inlet temperature (K)
T_a	ambient temperature (K)
T_{pm}	mean plate temperature (K)
T_{am}	mean air temperature (K)
T_w	wall temperature (K)
T_m	bulk mean temperature (K)
U_L	overall heat loss coefficient ($W/m^2/K$)
v	velocity of air in the duct (m/s)
W	width of duct (m)

Dimensionless parameters

e/D	relative roughness height
f	friction factor
Nu	Nusselt number
Pr	Prandtl number
p/e	relative roughness pitch
R	roughness function
Re	Reynolds number
W/H	duct aspect ratio

Greek symbols

$(\tau\alpha)e$	effective transmittance–absorptance product
η_{th}	thermal efficiency
μ	dynamic viscosity ($N/s/m^2$)
μ_t	turbulent viscosity ($N/s/m^2$)
ρ	density of air (kg/m^3)
α	angle of attack (degree)
ε	dissipation rate
ω	specific dissipation rate
δ	transition sub-layer thickness (m)
κ	turbulence kinetic energy (m^2/s^2)
Γ	molecular thermal diffusivity
Γ_t	turbulent thermal diffusivity

Subscripts

a	ambient
am	air mean
f	fluid (air)
i	inlet
m	mean
o	outlet
pm	plate mean
s	smooth
t	turbulent
w	wall

1. Introduction

The twenty-first century is forming into the perfect energy storm. Rising energy prices, diminishing energy availability and security, and growing environmental concerns are quickly changing the global energy panorama. Energy and water are the keys to modern life and provide the basis necessary for sustained economic development. Industrialized societies have become increasingly dependent on fossil fuels for myriad uses. Modern conveniences, mechanized agriculture, and global population growth have only been made possible through the exploitation of inexpensive fossil fuels. Securing sustainable and future energy supplies will be the greatest challenge faced by all societies in this century. Due to a growing world population and increasing modernization, global energy demand is projected to more than double during the first half of the twenty-first century and to more than triple by the end of the century. Presently, the world's population is nearly 7 billion, and projections are for a global population approaching 10 billion by midcentury. Future energy demands can only be met by introducing an increasing percentage of alternative fuels. Incremental improvements in existing energy networks will be inadequate to meet this growing energy demand. Due to dwindling reserves and ever-growing concerns over the impact of burning carbon fuels on global climate change, fossil fuel sources cannot be exploited as in the past. Finding sufficient supplies of clean and sustainable energy for the future is the global society's most daunting challenge for the twenty-first century. The future will be a mix of energy technologies with renewable sources such as solar, wind, and biomass playing an increasingly important role in the new global energy economy. The key question is: how long it will take for this sustainable energy changeover to occur? And how much environmental, political, and economic damage is acceptable in the meantime? If the twenty-first century sustainable energy challenge is not met quickly, many less-developed countries will suffer major famines and social instability from rising energy prices. Ultimately, the world's economic order is at stake. Approximately one-third of the world's population lives in rural regions without access to the electric grid, and about half of these same people live without access to safe and clean water. Solar energy is unique in that it can easily provide electricity and purified water for these people today with minimal infrastructure requirements by using local energy resources that promote local economic development [1–5].

Solar air heaters, because of their simple in design, are cheap and most widely used collection devices of solar energy. It is one of the basic equipment through which solar energy is converted into thermal energy. The main applications of solar air heaters are space heating, seasoning of timber, curing of industrial products and these can also be effectively used for curing/drying of concrete/clay building components. A conventional solar air heater generally consists of an absorber plate, a rear plate, insulation below the rear

plate, transparent cover on the exposed side, and the air flows between the absorbing plate and rear plate. A solar air heater is simple in design and requires little maintenance. However, the value of the heat transfer coefficient between the absorber plate and air is low and this results in a lower efficiency [6,7].

CFD is a science that can be helpful for studying fluid flow, heat transfer, chemical reactions etc. by solving mathematical equations with the help of numerical analysis. It is equally helpful in designing a solar air heater system from scratch as well as in troubleshooting/optimization by suggesting design modifications. CFD employs a very simple principle of resolving the entire system in small cells or grids and applying governing equations on these discrete elements to find numerical solutions regarding pressure distribution, temperature gradients, flow parameters and the like in a shorter time at a lower cost because of reduced required experimental work [8–13].

A lot of experimental studies have been carried out to evaluate performance of solar air heater but very few attempts of CFD investigation have been made so far due to complexity of flow pattern and computational limitations. With the development of computer, hardware and numerical methodology, applications of CFD are being used to carry out critical investigations in the field of solar air heaters. One of the great challenges in the design of a solar air heater using CFD approach is the selection of appropriate turbulence model. The decision about an appropriate turbulence model chosen in a CFD computation is not easy. In this article a CFD investigation is also carried out to select best turbulence model for the design of a solar air heater. The main objectives of this article are:

1. To present a detailed review of the literature that deals with the application of CFD in the design of solar air heater.
2. To examine the predictive ability of five different turbulence models such as: Standard k–ε model, Renormalization-group k–ε model, Realizable k–ε model, Standard k–ω and Shear Stress Transport k–ω model using commercial CFD software ANSYS FLUENT v12.1.

2. Thermal performance of solar air heater

Performance of any system represents the degree of utilization of input to the system. It is required to analyze thermal and hydraulic performance of a solar air heater for making an efficient design of such type of a system. Thermal performance concerns with heat transfer process within the collector and hydraulic performance concerns with pressure drop in the duct. A conventional solar air heater (Fig. 1) is considered for brief analysis of thermal and hydraulic performance in the following sub-sections. Design and construction details of such type of conventional system are described by Garg and Prakash [14].

2.1. Thermal performance

Thermal performance of a solar air heater can be computed with the help of Hottel–Whillier–Bliss equation reported by Duffie and Beckman [15].

$$Q_u = A_C \; F_R \,[\, I(\tau\alpha)_e - U_L(T_i - T_a) \,] \tag{1}$$

or

$$q_u = \frac{Q_u}{A_c} = F_R \left[\, I(\tau\alpha)_e - U_L(T_i - T_a) \,\right] \tag{2}$$

The rate of valuable energy gain by flowing air in the duct of a solar air heater can also be calculated from the following equation:

$$Q_u = \dot{m}\; c_p\,(T_o - T_i) = hA_c\,(T_{pm} - T_{am}) \tag{3}$$

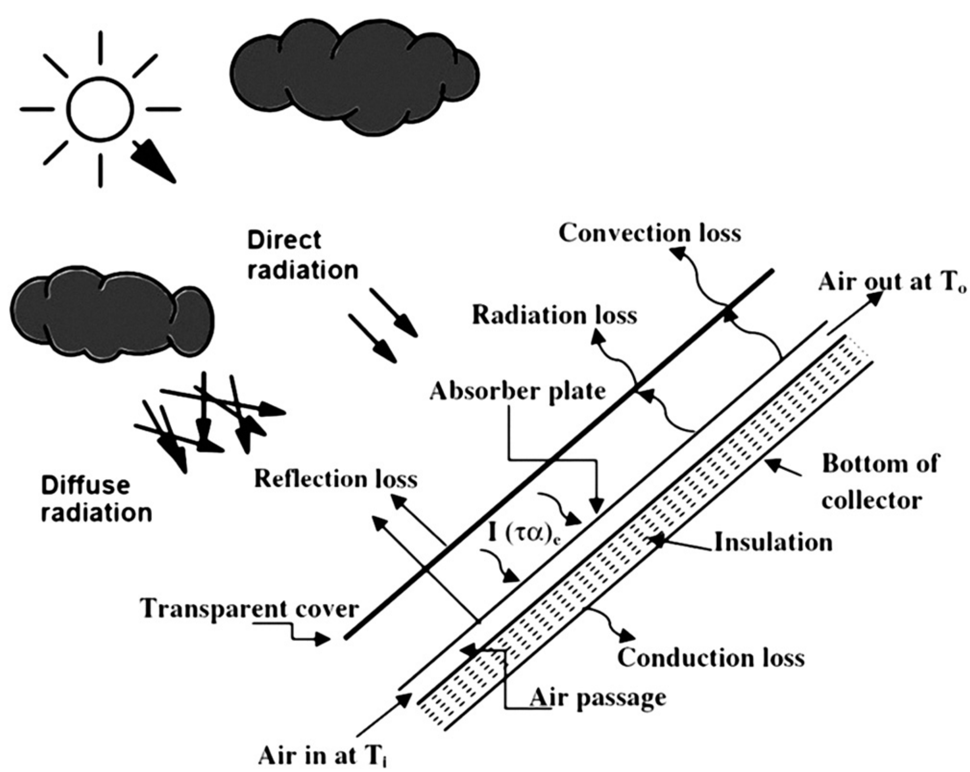


Fig. 1. Conventional solar air heater.

The value of heat transfer coefficient (h) can be increased by various active and passive augmentation techniques. It can be represented in non-dimensional form of Nusselt number (Nu).

$$Nu = hl/k \tag{4}$$

Further, thermal efficiency of a solar air heater can be expressed by the following equation;

$$\eta_{th} = \frac{q_u}{I} = F_R\left[(\tau\alpha)_e - U_L(T_i - T_a)/I\right] \tag{5}$$

2.2. Hydraulic performance

Hydraulic performance of a solar air heater concerns with pressure drop (ΔP) in the duct. Pressure drop accounts for energy consumption by blower to propel air through the duct. The pressure drop for fully developed turbulent flow through duct with $Re < 50{,}000$ is given as follows equation:

$$\Delta P = \frac{2f\rho l v^2}{D} \tag{6}$$

where

$$f = 0.079\, R_e^{-0.25} \tag{7}$$

2.3. Thermo-hydraulic performance

It is necessary that while evaluating the performance of a solar air heater with respect to the enhancement of thermal gain, the energy spent in propelling air should also be taken into account. It is desirable that design of solar air heater should be made in such a way that it should transfer maximum heat energy to the flowing fluid with minimum consumption of blower energy. Therefore in order to analyze overall performance of a solar air heater, thermo-hydraulic performance should be evaluated by considering thermal and hydraulic characteristics of the collector simultaneously. Thermo-hydraulic performance of a solar air heater is given by the following index

$$\text{Thermohydraulic performance} = \frac{Nu/Nu_s}{(f/f_s)^{1/3}} \tag{8}$$

3. Method of prediction

There are basically three approaches or methods that can be used to solve a problem of fluid flow and heat transfer. These approaches are:

1. Experimental
2. Theoretical
3. Computational (CFD)

3.1. Experimental approach

The most reliable information about a physical process is often given by actual measurement. An experimental approach involving full-scale equipment can be used to predict how identical copies of the equipment would perform under the same conditions. Such full scale tests are, in most cases, prohibitively expensive and often impossible. The alternative then is to perform experiments on small-scale models. The resulting information however must be extrapolated to full scale, and general rules for doing this are often unavailable. Further, the small-scale models do not always simulate all the features of the full-scale equipment; frequently, important features such as combustion or boiling are omitted from the model tests. This further reduces the usefulness of the test results. Finally it must be remembered that there are serious difficulties of measurement in many situations, and that the measuring instruments are not free from errors [16].

3.2. Theoretical approach

A theoretical prediction works out the consequences of a mathematical model, rather than those of an actual physical model. For the physical processes of interest, the mathematical model mainly consists of a set of differential equations. If the methods of classical mathematics were to be used for solving these equations, there would be little hope of predicting many phenomena of practical interest. In the theoretical approach simplifying assumptions are used in order to make the problems tractable [17].

3.3. Computational approach

Computational fluid dynamics or CFD is the analysis of systems involving fluid flow, heat transfer and associated phenomena such as chemical reactions by means of computer-based simulation. The technique is very powerful and spans a wide range of industrial and non-industrial application areas. Some examples are:

- aerodynamics of aircraft and vehicles: lift and drag
- hydrodynamics of ships
- power plant: combustion in internal combustion engines and gas turbines
- turbo machinery: flows inside rotating passages, diffusers etc.
- electrical and electronic engineering: cooling of equipment including microcircuits
- chemical process engineering: mixing and separation, polymer moulding
- external and internal environment of buildings: wind loading and heating/ventilation
- marine engineering: loads on off-shore structures
- environmental engineering: distribution of pollutants and effluents
- hydrology and oceanography: flows in rivers, estuaries, oceans
- meteorology: weather prediction
- biomedical engineering: blood flows through arteries and veins

The equations governing the fluid flow are the continuity (conservation of mass), the Navier–Stokes (balance of momentum), and the energy (conservation of energy) equations. These equations form a system of coupled non-linear partial differential equations (PDEs). Because of the coupled nature of the equations and the presence of non-linear terms, the fluid flow equations are generally not amenable to analytical method of obtaining the solution. In general, closed form analytical solutions are possible only if these PDEs can be made linear, either because non-linear terms naturally drop out (as in the case of parallel flows or flows that are inviscid and irrotational everywhere) or because the nonlinear terms are small compared to other terms so that they can be neglected (e.g., creeping flows, small amplitude sloshing of liquid etc.). If the non-linearities in the governing PDEs cannot be neglected, which is often the case for most engineering flows, one normally has to resort to numerical methods to obtain solutions.

CFD is the art of replacing the differential equations governing the Fluid Flow, with a set of algebraic equations (this process is called the discretization), which in turn can be solved with the aid of a digital computer to get an approximate solution. The commonly used discretization methods in CFD analysis are the finite difference method (FDM), the finite volume method (FVM), the finite element method (FEM), and the boundary element method (BEM). Some special cases of flow problems can also be solved using nonstandard method like, boundary integral methods, spectral methods, and pseudo-spectral methods. From the 1960s onwards the aerospace industry has integrated CFD techniques into the design, R&D and manufacture of aircraft and jet engines.

More recently the methods have been applied to the design of internal combustion engines, combustion chambers of gas turbines and furnaces. Furthermore, motor vehicle manufacturers now routinely predict drag forces, under-bonnet air flows and the in-car environment with CFD. Increasingly CFD is becoming a vital component in the design of industrial products and processes. The ultimate aim of developments in the CFD field is to provide a capability comparable with other CAE (computer-aided engineering) tools such as stress analysis codes. The main reason why CFD has lagged behind is the tremendous complexity of the underlying behaviour, which precludes a description of fluid flows that is at the same time economical and sufficiently complete. The availability of affordable high-performance computing hardware and the introduction of user-friendly interfaces have led to a recent upsurge of interest, and CFD has entered into the wider industrial community since the 1990s.

There are several unique advantages of CFD over experiment-based approaches to fluid systems design:

- substantial reduction of lead times and costs of new designs
- ability to study systems where controlled experiments are difficult or impossible to perform (e.g., very large systems)
- ability to study systems under hazardous conditions at and beyond their normal performance limits (e.g., safety studies and accident scenarios)
- practically unlimited level of detail of results.

CFD codes are structured around the numerical algorithms that can tackle fluid flow problems. In order to provide easy access to their solving power all commercial CFD packages include sophisticated user interfaces to input problem parameters and to examine the results. Hence all codes contain three main elements: (i) a pre-processor, (ii) a solver and (iii) a post-processor. We briefly examine the function of each of these elements within the context of a CFD code.

3.3.1. Pre-processor

Pre-processing consists of the input of a flow problem to a CFD program by means of an operator-friendly interface and the subsequent transformation of this input into a form suitable for use by the solver. The user activities at the pre-processing stage involve:

- Definition of the geometry of the region of interest: the computational domain
- Grid generation—the sub-division of the domain into a number of smaller, non-overlapping sub-domains: a grid (or mesh) of cells (or control volumes or elements)
- Selection of the physical and chemical phenomena that need to be modelled
- Definition of fluid properties
- Specification of appropriate boundary conditions at cells which coincide with or touch the domain boundary

Solution to a flow problem (velocity, pressure, temperature etc.) is defined at nodes inside each cell. The accuracy of a CFD solution is governed by the number of cells in the grid. In general, the larger the number of cells, the better the solution accuracy. Both the accuracy of a solution and its cost in terms of necessary computer hardware and calculation time are dependent on the fineness of the grid. Optimal meshes are often non-uniform: finer in areas where large variations occur from point to point and coarser in regions with relatively little change. Efforts are under way to develop CFD codes with a self-adaptive meshing capability. Ultimately such programs will automatically refine the grid in areas of rapid variations. A substantial amount of basic development work still needs to be done before these techniques are robust enough to be incorporated into commercial CFD codes. At present it is still up to the skills of the CFD user to design a grid that is a suitable compromise between desired accuracy and solution cost.

3.3.2. Solver

There are three distinct streams of numerical solution techniques: finite difference, finite element and spectral methods. We are solely concerned with the finite volume method, a special finite difference formulation that is central to the most well-established CFD codes: CFX/ANSYS, FLUENT, PHOENICS and STAR-CD. In outline the numerical algorithm consists of the following steps:

- Integration of the governing equations of fluid flow over all the (finite) control volumes of the domain
- Discretization—conversion of the resulting integral equations into a system of algebraic equations
- Solution of the algebraic equations by an iterative method

The first step, the control volume integration, distinguishes the finite volume method from all other CFD techniques. The resulting statements express the exact conservation of relevant properties for each finite size cell. This clear relationship between the numerical algorithm and the underlying physical conservation principle forms one of the main attractions of the finite volume method and makes its concepts much simpler to understand by engineers than the finite element and spectral methods. The conservation of a general flow variable φ, e.g., a velocity component or enthalpy, within a finite control volume can be expressed as a balance between the various processes tending to increase or decrease it. In words we have:

$$\begin{bmatrix}\text{Rate of change}\\ \text{of } \Phi \text{ in the control}\\ \text{volume with respect}\\ \text{to time}\end{bmatrix} = \begin{bmatrix}\text{Net Rate of increase}\\ \text{of } \Phi \text{ due to convection}\\ \text{in to the control}\\ \text{volume}\end{bmatrix} + \begin{bmatrix}\text{Net Rate of increase}\\ \text{of } \Phi \text{ due to diffusion}\\ \text{in to the control}\\ \text{volume}\end{bmatrix} + \begin{bmatrix}\text{Net Rate of creation}\\ \text{of } \Phi \text{ inside the}\\ \text{control volume}\end{bmatrix}$$

CFD codes contain discretization techniques suitable for the treatment of the key transport phenomena, convection (transport due to fluid flow) and diffusion (transport due to variations of Φ from point to point) as well as for the source terms (associated with the creation or destruction of Φ) and the rate of change with respect to time. The underlying physical phenomena are complex and non-linear so an iterative solution approach is required. The most popular solution procedures are by the TDMA (tri-diagonal matrix algorithm) line-by-line solver of the algebraic equations and the SIMPLE algorithm to ensure correct linkage between pressure and velocity. Commercial codes may also give the user a selection of further, more recent, techniques such as Gauss–Seidel point iterative techniques with multigrid accelerators and conjugate gradient methods.

3.3.3. Post-processor

As in pre-processing, a huge amount of development work has recently taken place in the post-processing field. Due to the increased popularity of engineering workstations, many of which have outstanding graphics capabilities, the leading CFD packages are now equipped with versatile data visualization tools. These include:

- Domain geometry and grid display
- Vector plots
- Line and shaded contour plots
- 2D and 3D surface plots

- Particle tracking
- View manipulation (translation, rotation, scaling etc.)
- Color PostScript output

More recently these facilities may also include animation for dynamic result display, and in addition to graphics all codes produce trusty alphanumeric output and have data export facilities for further manipulation external to the code. As in many other branches of CAE, the graphics output capabilities of CFD codes have revolutionized the communication of ideas to the non-specialist [18]. Table 1 shows the comparison of three approaches.

4. Applications of CFD in various aspects of solar air heaters

A lot of experimental and theoretical studies have been reported to evaluate performance of solar air heater. Kumar et al. [19] experimentally investigated heat transfer and friction characteristics of solar air heater by using discrete W-shaped roughness on one broad wall of solar air heater. The maximum enhancement of Nusselt number and friction factor as a result of providing artificial roughness was found to be 2.16 and 2.75 times that of smooth duct. Mittal et al. [20] presented a comparison of effective efficiency of solar air heaters having different types of geometry of roughness elements on the absorber plate. The effective efficiency was computed by using the correlations for heat transfer and friction factor developed by various investigators within the investigated range of operating and system parameters. Prasad and Saini [21] developed various design curves for artificially roughened solar air heater that gave the optimal thermo-hydraulic performance. Prasad and Saini [22] investigated the effect of relative roughness pitch (P/e) and relative roughness height (e/D) on the heat transfer coefficient and friction factor for fully developed turbulent flow in a solar air heater duct with small diameter protrusion wires on the absorber plate. It was found that for a given relative roughness pitch, both the Nusselt number and friction factor increased with increasing relative roughness height and for a given relative roughness height both the Nusselt number and friction factor decreased with increasing relative roughness pitch, but not in direct proportion. Aharwal et al. [23] carried out an experimental investigation of heat transfer and friction factor characteristics of a rectangular duct roughened with repeated square cross-section split-rib with a gap, on one broad wall arranged at an inclination with respect to the flow direction. The maximum enhancement in Nusselt number and friction factor was observed to be 2.59 and 2.87 times of that of the smooth duct respectively. The thermo-hydraulic performance parameter was found to be maximum for the relative gap width of 1.0 and the relative gap position of 0.25. Muluwork [24] carried out an experimental analysis of a solar air heater having V-shaped staggered discrete ribs on the absorber plate and reported that maximum heat transfer enhancement occurred at an angle of attack of 60°. Prasad and Mullick [25] utilized artificial roughness in a solar air heater duct in the form of small diameter wires to increase the heat transfer coefficient for relative roughness height and relative roughness pitch of 0.019 and 12.7, respectively. Gupta [26] investigated the effect of relative roughness height, angle of attack and Reynolds number on heat transfer and friction factor in rectangular duct having circular wire ribs on the absorber plate. The maximum enhancement of Nusselt number and friction factor as a result of providing artificial roughness was found to be 1.8 and 2.7 times that of smooth duct. Verma and Prasad [27] investigated the effect of geometrical parameters of circular wire ribs on heat transfer and friction factor. It was observed that the value of heat transfer enhancement factor varies from 1.25 to 2.08 within the range of parameters investigated. The value of optimal thermo-hydraulic performance was found to be about 71% corresponding to roughness Reynolds number of 24. Karwa [28] carried out a comparative experimental study of augmented heat transfer and friction in a rectangular duct of a solar air heater with rectangular cross-section ribs arranged in V-continuous and V-discrete pattern. The performance of V-down ribs was observed to be better than that of V-up ribs. Sahu and Bhagoria [29] experimentally investigated the effect of 90° broken ribs as roughness elements and found that thermal efficiency lies in the range of 51–83.5%. The maximum enhancement in heat transfer was reported at the pitch of 20 mm. Gupta et al. [30] investigated the effect of transverse and inclined wire roughness on fluid flow characteristics of a solar air heater. Authors reported that heat transfer coefficient of roughened duct using transverse wires fixed on absorber plate as roughness geometry can be improved by a factor of 1.8 times of the smooth duct at the cost of friction penalty. Saini and Saini [31] used expanded metal mesh as roughness geometry and obtained an enhancement of heat transfer coefficient and friction factor of the order 4 and 5 times over the smooth duct corresponding to an angle of attack of 61.9° and 72° respectively. Momin et al. [32] experimentally investigated the effect of geometrical parameters of V-shaped ribs on heat transfer and fluid flow characteristics of rectangular duct of solar air heater. The maximum enhancement of Nusselt number and friction factor as a result of providing artificial roughness was found to be 2.3 and 2.83 times that of smooth duct. Karwa et al. [33] performed an experimental investigation of heat transfer and friction in a high-aspect-ratio rectangular duct with repeated rectangular cross-section ribs on one broad wall in v-discrete and discontinuous patterns at different angles. The performance of V-down ribs was observed to be better than that of V-up ribs. Karwa et al. [34] carried out an experimental investigation of heat transfer and friction of rectangular solar air heater ducts roughened with chamfered ribs. The highest heat transfer rate and also the highest friction factor occurred for 15° chamfered ribs. The enhancement in the Stanton number was reported to be 65–90% while friction factor was found to be 2.68–2.94 times as compared to smooth duct. Bhagoria et al. [35] performed experiments to determine the effect of relative roughness pitch, relative roughness height and wedge angle on the heat transfer and friction factor in a solar air heater roughened duct having wedge shaped rib roughness. Statistical correlations for the Nusselt number and friction factor

Table 1
Comparison of different approaches.

Approach	Advantage	Disadvantage
Experimental	1. Capable of being most realistic	1. Equipment required 2. Scaling problems 3. Tunnel corrections 4. Measurement difficulties 5. Operating costs
Theoretical	1. Clean, general information, which is usually in formula form	1. Restricted to simple geometry and physics 2. Usually restricted to linear problems
Computational	1. No restriction to linearity 2. Complicated physics can be treated 3. Time evolution of flow can be obtained	1. Truncation errors 2. Boundary conditions problems 3. Computer costs

were developed in terms of geometrical parameters of the roughness elements and the flow Reynolds number. Maximum heat transfer occurred for relative roughness pitch of 7.57. Wedge angle of 10° gave maximum enhancement of heat transfer. Saini and Saini [36] studied the effect of arc shaped ribs on the heat transfer coefficient and friction factor of rectangular solar air heater ducts. Enhancement of heat transfer and friction factor was reported to be of order 3.6 and 1.75 times respectively over smooth solar air heater duct for relative arc angle value of 0.333 and relative roughness height value of 0.042. Saini and Verma [37] investigated the effect of roughness and operating parameters on heat transfer and friction factor in a roughened duct provided with dimple-shape roughness geometry for the range of Reynolds number from 2000 to 12,000, relative roughness height from 0.018 to 0.037 and relative roughness pitch from 8 to 12. The maximum value of the heat transfer was found to be corresponding to relative roughness height of 0.037 and relative roughness pitch of 10. Karmare and Tikekar [38] performed an experimental investigation of heat transfer to the airflow in the rectangular duct of an aspect ratio 10:1. The top wall surface was made rough with metal ribs of circular cross section in staggered manner to form defined grid. The roughened wall was uniformly heated and the other walls were insulated. The effect of relative roughness height of grit, relative roughness pitch of grit and relative length of grit on the heat transfer coefficient and friction factor were investigated by authors. Kumar et al. [39] carried out an experimental investigation to determine the heat transfer distributions in solar air heater having its absorber plate roughened with discrete w-shaped ribs. It was reported that thermal performance of the roughened duct was found to be 1.2–1.8 times the smooth channel for range of parameters investigated. Jaurker et al. [40] investigated the effect of relative roughness pitch, relative roughness height and relative groove position on the heat transfer coefficient and friction factor of rib-grooved artificial roughness. The maximum heat transfer was obtained for a relative roughness pitch of about 6, and it was decreased on either side of the relative roughness pitch. The optimal condition for heat transfer was found at a groove position to pitch ratio of 0.4 as compared to the smooth duct. As compared to smooth surface, the presence of rib grooved artificial roughness increases the Nusselt number up to 2.7 times, while the friction factor raises up to 3.6 times in the range of parameters investigated. Layek et al. [41] investigated heat transfer and friction characteristics of repeated integral transverse chamfered rib-groove roughness. Authors reported that Nusselt number and friction factor was increased by 3.24 times and 3.78 times respectively as compare to smooth duct. Maximum enhancement of Nusselt number and friction factor was obtained corresponding to relative groove position of 0.4. Varun et al. [42] performed an experimental study on heat transfer and friction characteristics by using a combination of inclined and transverse ribs on the heated plate of a solar air heater duct. The best thermal performance was reported for relative roughness pitch value of 8 and relative roughness height value of 0.030. Lanjewar et al. [43] carried out an experimental investigation of heat transfer and friction factor characteristics of rectangular duct roughened with W-shaped ribs on its underside on one broad wall arranged at an inclination with respect to flow direction. Maximum enhancement of Nusselt number and friction factor as a result of providing artificial roughness was found to be, respectively, 2.36 and 2.01 times that of smooth duct for an angle of attack of 60°. Maximum thermo-hydraulic performance occurred at an angle of attack of 60°. Correlations were developed for heat transfer coefficient and friction factor for roughened duct. Varun et al. [44], Hans et al. [45], Bhushan and Singh [46] and Kumar et al. [47] also reported different investigations on roughness elements of different shapes, sizes and orientations carried out in solar air heater in order to obtain an optimum arrangement of roughness element geometry.

The literature survey reveals that a lot of experimental and theoretical studies have been reported to evaluate performance of solar air heater, but literature search also reveals in this area that few CFD studies have been done on the performance evaluation of solar air heater.

Arulanandam et al. [48] investigated heat transfer and flow characteristics for a representative element of an unglazed transpired-plate absorber with holes in a square pitch arrangement under no wind conditions using CFD. The study was completed using TASC flow, a state-of-the-art CFD code. A mathematical model was developed with the relevant boundary conditions and interfacial (solid–fluid) conditions specified. It is reported that if transpired-plate absorbers were to be made from lower conductivity materials, such as plastics, acceptable efficiencies could still be achieved. Fig. 2(a) shows a sketch of the transpired plate with circular holes on a square pitch arrangement in zero wind and Fig. 2(b) shows the computational domain used for CFD analysis. The results obtained from CFD approach were reported to be closer to the experimental results.

Ammari [49] proposed a CFD model for computing the thermal performance of a single pass flat-plate solar air heater. Proposed solar air heater with slats is shown schematically in Fig. 3. Air channels were formed by providing metal slats running along the circulated air passage linking the absorber plate by the bottom

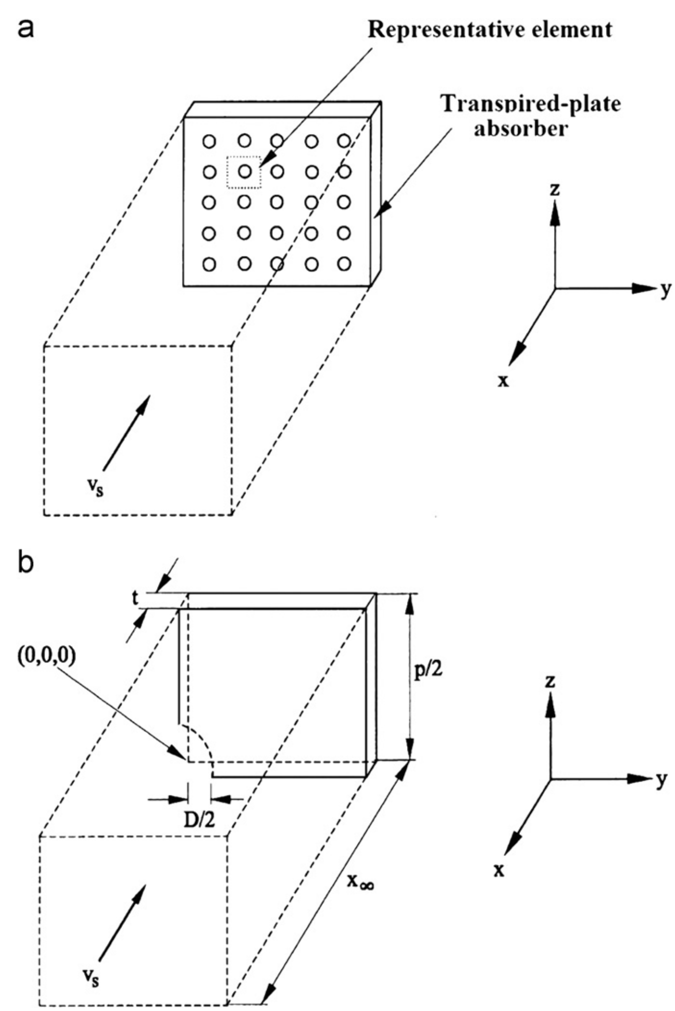


Fig. 2. (a) Sketch of the representative elements of the absorber plate and (b) The computational domain.

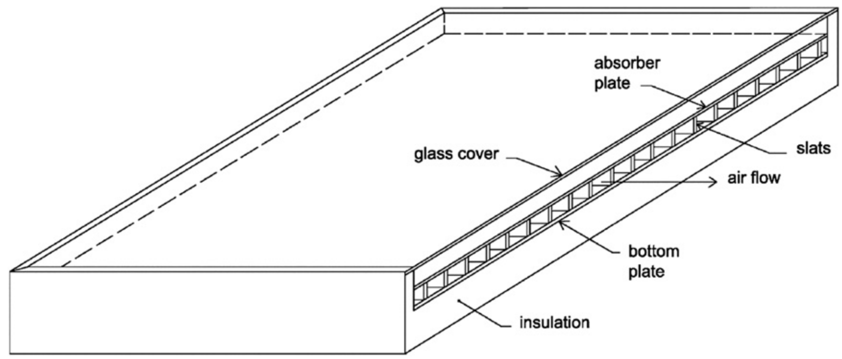


Fig. 3. Flat-plate solar air heater with slats.

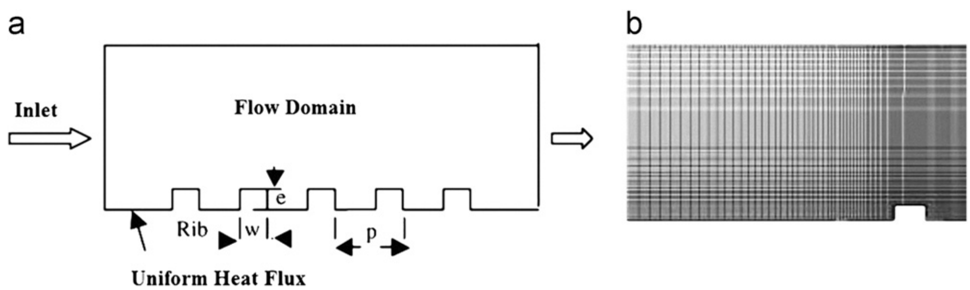


Fig. 4. (a) Solution domain and (b) rectangular meshing.

one in an endeavor to enhance the thermal efficiency of the solar air collector. A computer code based on FORTRAN was developed to solve for the governing energy equations to estimate the mean temperatures of the collector. The effect of volume airflow rate, collector length, and spacing between the absorber and bottom plates on the thermal performance of the present solar air heater was investigated. Predicted temperatures and efficiencies of the two air heaters were presented in which the proposed model heater with the slats showed a noticeable improvement in performance over that of the most common type conventional heater. A numerical comparison of the present design with the most common type of solar air heaters was conducted. The CFD results showed good agreements with experimental results.

Chaube et al. [50] performed a computational analysis of heat transfer augmentation and flow characteristics due to artificial roughness in the form of ribs on a broad heated wall of a rectangular duct of a solar air heater for turbulent flow (Reynolds number range of 3000–20,000). A 2D analysis of heat transfer and fluid flow through an artificially roughened solar air heater was carried out using commercially available CFD software, FLUENT 6.1. Shear Stress Transport k–ω turbulence model was selected by comparing the predictions of different turbulence models with experimental results available in the literature. The results obtained from CFD approach were reported to be closer to the experimental results. The solution domain and rectangular meshing used in CFD simulation are shown in Fig. 4(a) and (b). Based on the computational results following conclusions were drawn: (1) It was observed that the 2D analysis model itself yields results which were closer to the experimental ones as compared to 3D models (Fig. 5). The 3D model required much higher memory and computational time compared to 2D ones. Hence, it was sufficient to employ a simpler 2D model which was more economical with the memory and computational time requirements. (2) In the inter-rib region, the model predicted well near the central high heat transfer area but it under predicted around ribs. (3) The peaks of local heat transfer were found at the reattachment points. (4) The turbulence intensity was found maximum at the peak of the local heat transfer coefficient in the inter-

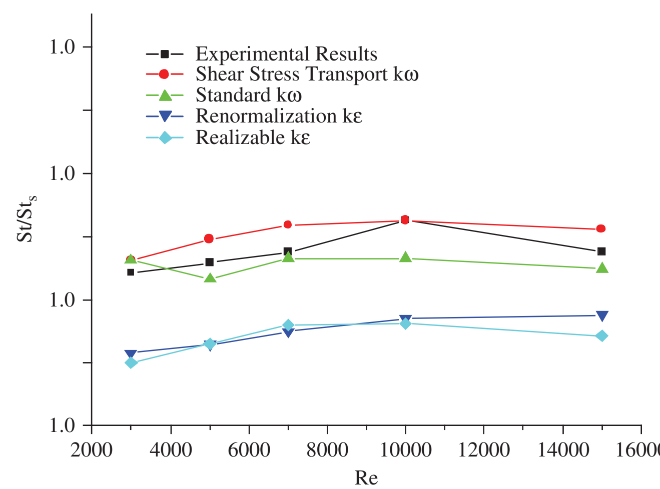


Fig. 5. Comparison between CFD predictions with experimental results.

rib regions. (5) The peaks of the local heat transfer coefficient and the reattachment lengths decreased stream wise in the successive inter-rib regions up to 3–4 ribs and then the distribution became periodic with peak values and the reattachment lengths remained unchanged. (6) The highest heat transfer was achieved with chamfered ribs but the best performance index was found with rectangular rib of size 3×5 mm.

Chaube et al. [51] carried out a 2D computational analysis to assess the comparative performance of the absorber plate of a solar air heater with different roughness elements using commercial software package FLUENT 6.1. The assessment was based on heat transfer enhancement with minimum pressure penalty. Ten different ribs shape viz. rectangular, square, chamfered, triangular, semicircle etc. (Fig. 6) were investigated at the Reynolds number range from 3000 to 20,000, in which solar air heaters normally operate. The SST k–ω turbulence model was selected by comparing the predictions of different turbulence

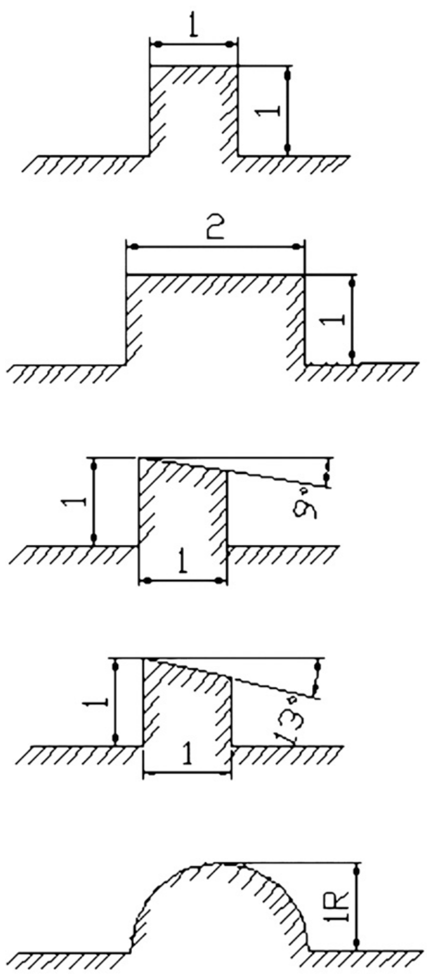


Fig. 6. Different roughness elements.

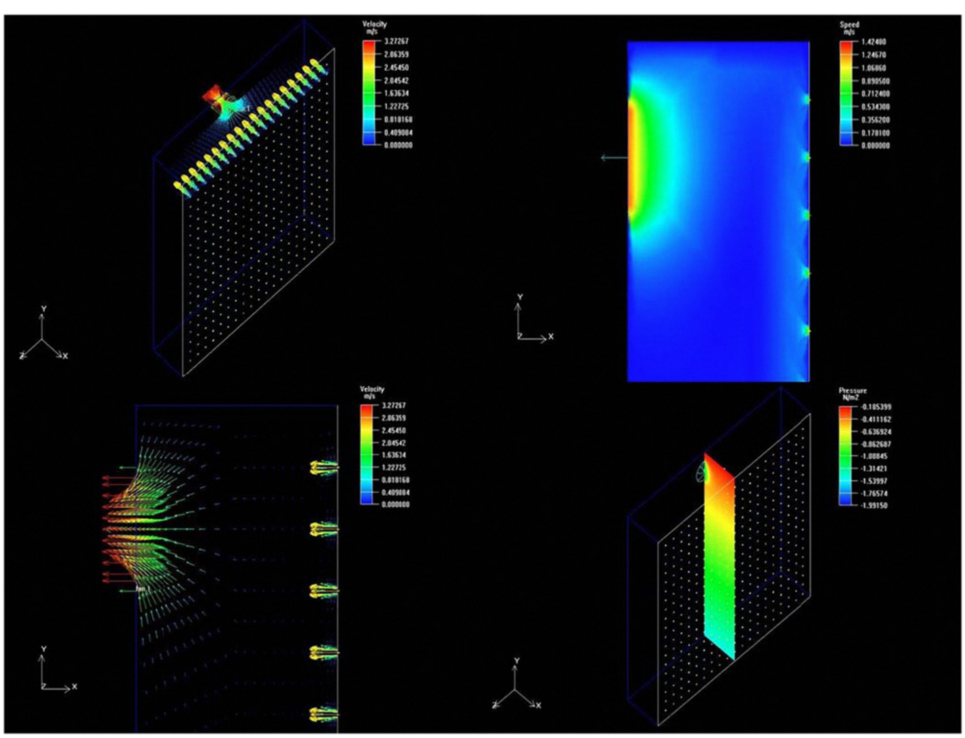


Fig. 7. Simulation of different flow rate.

models with experimental results available in the literature. Based on the CFD results following conclusions were drawn: (1) The Shear Stress Transport $k-\omega$ turbulence model predicted very close results to the experimental results, which yield confidence in the predictions done by CFD analysis. (2) In transitionally rough flow a substantial enhancement in heat transfer was found along with increase in friction factor, but in fully rough flow a marginal enhancement in heat transfer over that in the transitionally rough flow was found with sharp increase (more than double in comparison to transitionally rough flow regime) in friction factor. (3) There was a great influence of reattachment of flow on convective heat transfer coefficient. (4) For rectangular ribs, there was an optimum width of rib at which it gave maximum heat transfer with minimum pressure drop penalty. (5) Chamfered ribs were not much effective because although they gave small enhancement in heat transfer but at the cost of steep rise in friction factor. (6) The thermo-hydraulic analysis for constant pumping power showed that rectangular rib (1 mm × 2 mm) gave the best performance in comparison to other shapes under consideration.

Wang et al. [52] made comparative analysis of several types of solar air collector with numerical simulation tools, got several important conclusions, validated the advantages of unglazed transpired solar air collector UTC in ventilation preheating field and investigated the flow rate and radiant intensity's effort to the effectiveness. They observed that CFD tools had its own advantages in the field of solar air collector research; it was a powerful assistant tool for researching and was worth to be applied in more abroad fields. Based on CFD study authors reported: (1) Under fresh air operating mode, UTC had higher effectiveness than flat collector and unglazed collector, and could be further improved. (2) As the flow rate increased, the temperature of heated air decreased and the effectiveness increased (Fig. 7). (3) As the radiant intensity increased, the temperature of heated air increased, but the effectiveness had almost no change.

Varol and Oztop [53] carried out a numerical study to investigate natural convection heat transfer and flow field inside a different shaped inclined collectors such as flat and wavy collector (Fig. 8). A comparison was performed in these collectors from the heat transfer point of view. CFDRC commercial CFD code was used to simulate the laminar flow and thermal field. The main purpose of this numerical work was to compare the heat transfer rate in flat and wavy collectors. Based on CFD simulations following conclusions were made: (1) Natural convection heat transfer and fluid flow was strongly affected by the shape and inclination angle of the collector. (2) In all cases, more heat transfer was obtained in the case of wavy collector than that of flat collector. (3) There could be an optimum solution for the governing parameters which was effective on natural convection but it was out of the scope of the study. (4) Variation of local Nusselt number was almost linear for flat collector. (5) With the same aspect ratio, mean Nusselt number increased with the decreasing wave length. (6) In wavy collectors, the mean Nusselt number decreased with the increasing inclination angle. On the contrary of flat collectors, the highest Rayleigh number was obtained at the highest inclination angle which was the most important result of this numerical work.

Kumar and Saini [54] carried out a CFD based analysis of fluid flow and heat transfer characteristics of a solar air heaters having roughened duct provided with artificial roughness in arc shaped geometry (Fig. 9). The heat transfer and flow analysis of the chosen roughness element were carried out using 3D models. The ribs were provided on the absorber plate whereas other sides of the duct were kept smooth. FLUENT 6.3.26 commercial CFD code was used for simulation. Different Turbulence Models namely Shear Stress Transport $k-\omega$, Standard $k-\varepsilon$, Renormalization–group (RNG) $k-\varepsilon$ and Realizable $k-\varepsilon$ were tested for smooth duct having same cross-section of roughened duct in order to find out the validity of the models. The results obtained by different models were compared with Dittus–Boelter empirical correlation for Nusselt number. Based on the computational results following conclusions were drawn: (1) Nusselt number was found to increase with increase in Reynolds number whereas friction factor was found to decrease with increase in Reynolds number for all combinations of relative roughness height (e/D) and



Fig. 9. Solution domain for CFD analysis.

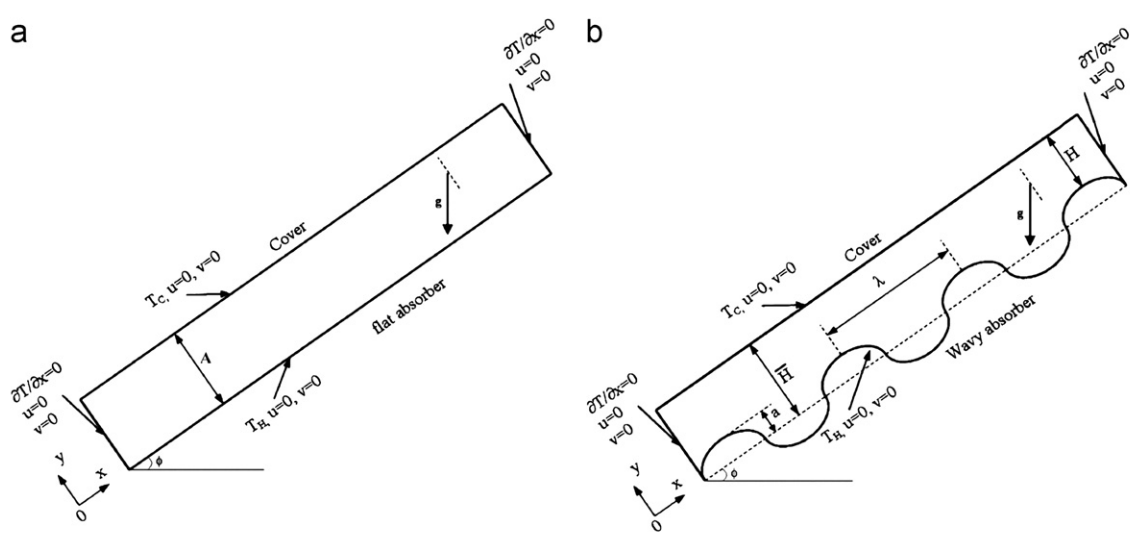


Fig. 8. Schematic models: (a) inclined flat collector and (b) inclined wavy collector.

relative arc angle (α/90). (2) CFD results were validated for smooth duct and different CFD model results were compared with Dittus–Boelter empirical relationship for smooth duct. (3) Among all the models used, Renormalization-group (RNG) k–ε model results were found to have good agreement. (4) Overall enhancement ratio with a maximum value of 1.7 was found for the roughness geometry corresponding to relative arc angle (α/90) of 0.333 and relative roughness height (e/D) of 0.0426 for the range of parameters considered.

Karmare and Tikekar [55] performed a CFD simulation of fluid flow and heat transfer in a solar air heater duct with metal grit ribs as roughness elements employed on one broad wall of a solar air heater. The circular, triangular and square shape rib grits (Fig. 10) with the angle of attack of 54°, 56°, 58°, 60° and 62° were tested for the same Reynolds number. The broad wall was subjected to uniform heat flux. The system and operating parameters studied were: e/D=0.044, P/e=17.5 and l/s=1.72, for the Reynolds number range 3600–17,000. To validate CFD results, experimental investigations were carried out in the laboratory. The major findings of the study were: (1) The CFD results gave the good agreements with experimental results. (2) Artificial roughness on the underside of the absorber plate of the solar air heater enhanced the rate of heat transfer from the absorber plate to the flowing air. (3) Amongst the different shape and orientations analyzed, the absorber plate of square cross-section rib with 58° angle of attack gave the best possible results. (4) The percentage increase in the heat transfer for 58° rib inclination plate over smooth plate was found to be about 30%.

Soi et al. [56] presented a CFD based investigation of heat transfer and friction characteristics of artificially roughened duct of a solar air heater (Fig. 11). K-shaped (combination of transverse and V-up) roughness geometry was used as an artificial roughness. 2D flow analysis of heat transfer and fluid flow through a rectangular duct roughened with K-shaped ribs were carried out using flow simulation module available in SolidWorks software of version 2010. 2D computational domain and grid were selected.

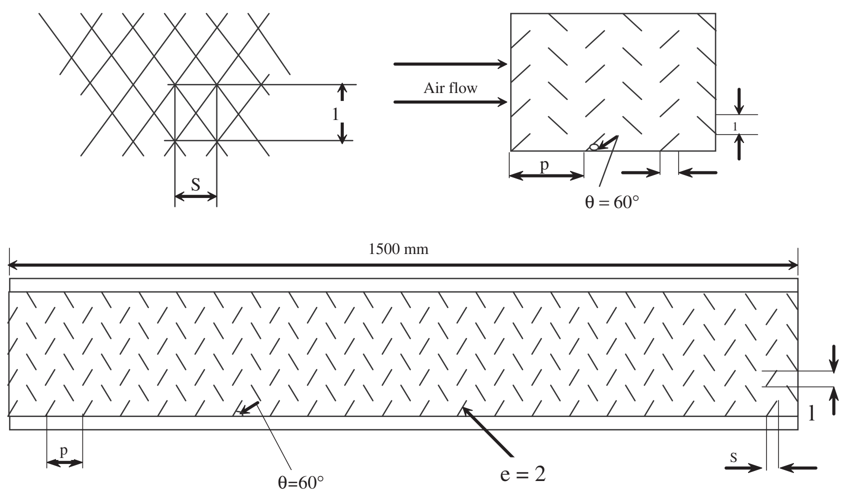


Fig. 10. Geometry of roughened surface collector plate.

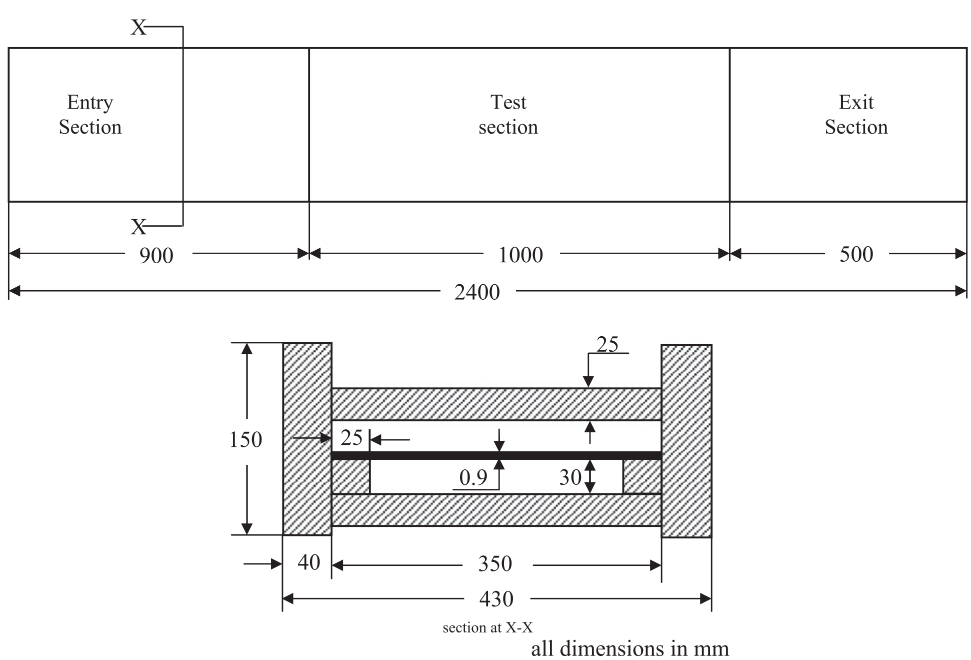


Fig. 11. Schematic of CFD model of solar air heater duct.

Non-uniform meshing was generated over the duct. FLUENT 6.3.26 commercial CFD code was used for simulation. Correlations for Nusselt number and friction factor were also developed corresponding to CFD data using SigmaPlot software. The major findings of the study were: (1) For a given type of artificial roughness, Nusselt number increased with an increase in Reynolds number for smooth as well as roughened plate. (2) With an increase in relative roughness pitch from 7.5 to 8.3, Nusselt number increased and was found maximum at P/e of 8.3. (3) Friction factor decreased with the increase of Reynolds number. (4) For a given value of relative roughness pitch (P/e) the friction factor decreased with increase of Reynolds number 5. A percentage deviation between CFD and predicted values of Nusselt number and friction factor for K-shaped ribs was found $\pm 15\%$ and $\pm 20\%$ respectively.

Giri [57] carried out a computational analysis of heat transfer and flow characteristics in a solar air heater having artificial roughness in the form of different types of ribs (square, triangular, chamfered and semicircular) on the absorber plate. CFD investigations were carried out for a range of Reynolds number from 3000 to 15,000 and relative roughness pitch from 5 to 20. In this study CFD code FLUENT 6.3.26 was used to perform a numerical simulation for reattachment point to enhance turbulent heat transfer. In this study Reynolds-Averaged Navier–Stokes analysis was used as a numerical technique and the RNG k–ε model with near-wall treatment as a turbulence model. The results were validated by comparing with existing experimental. Following conclusions were drawn from this CFD simulation: (1) The RNG k–ε model gave good results for the prediction of heat transfer and friction characteristics in high aspect ratio rib roughened rectangular duct. (2) It was observed that the 2D analysis model itself yields results, which were closer to the experimental ones as compared to 3D models. The 3D model required much higher memory and computational time compared to 2D ones. It might be because of negligible effect of secondary flow in transverse ribbed duct surface. Hence, it was sufficient to employ a simpler 2D model which was more economical with the memory and computational time requirement. (3) In the inter-rib region, the model predicted well near the central high heat transfer area but it under predicted around ribs. (4) The peaks of local heat transfer were found at the reattachment points. (5) The turbulence intensity was found maximum at peak of the local heat transfer coefficient in the inter-rib regions. (6) Chamfered shape ribs gave highest heat transfer enhancement. (7) CFD results also predicted that Nusselt number increased as ribs spacing increases. (8) Thermal performance decreased as Reynolds number increased. (9) Chamfered shape ribs gave minimum friction as compared to other ribs geometries (Fig. 12). (10) Solar air heater duct with Chamfered ribs gave maximum heat transfer enhancement with minimum friction factor hence better thermal hydraulic performance.

Rajput [58] performed a CFD simulation of heat transfer and fluid flow behavior in a rectangular duct of solar air heater with inverted U-type turbulator roughened ribs mounted on one of the principal wall (solar plate). CFD code FLUENT 6.3.26 was used to perform a numerical simulation. The Reynolds-Averaged Navier–Stokes analysis was used as a numerical technique and the k–ε turbulence model with near-wall treatment as a turbulence model (Fig. 13). The results were validated by comparing with existing experimental data. The major findings of the study were: (1) Provision of ribs completely obstructed the viscous sub-layer adjacent to the hot wall, which generated eddies/recirculation zones upstream and downstream, Eddies not only reduced the heat transfer but also increased the pressure drop. With opening the passage downstream the rib, intensity of eddies formation can be reduced. A thin inclined U-turbulator geometry with a passage underside can definitely prevent the formation of eddies and also

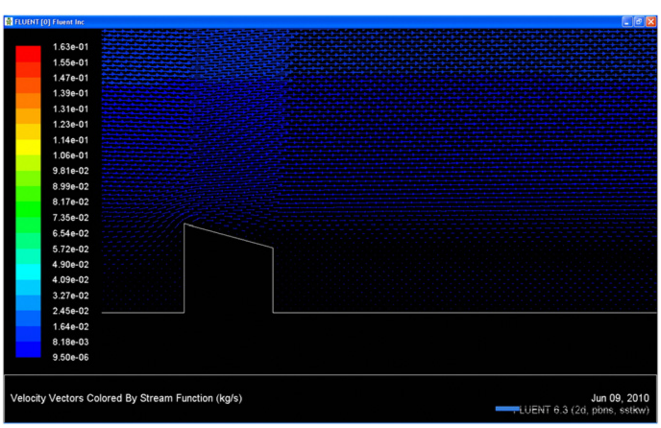


Fig. 12. Velocity profile for chamfered rib.

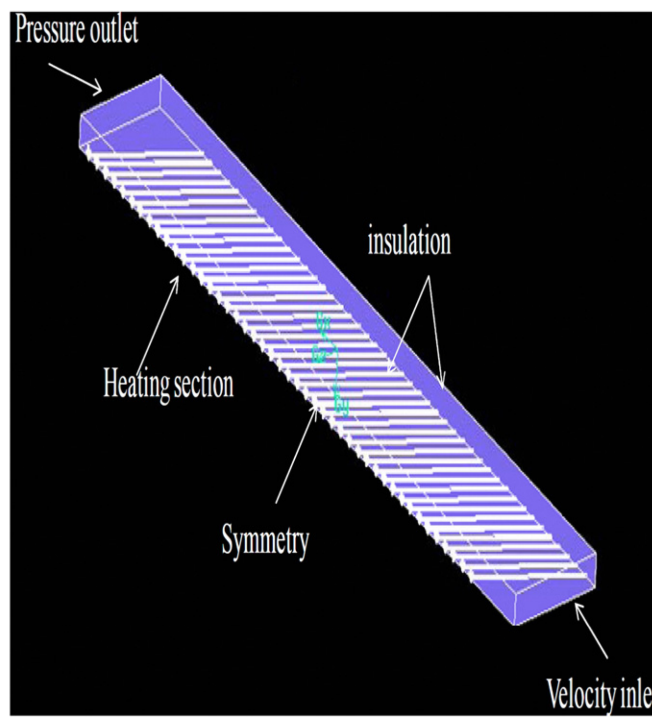


Fig. 14. The computational domain.

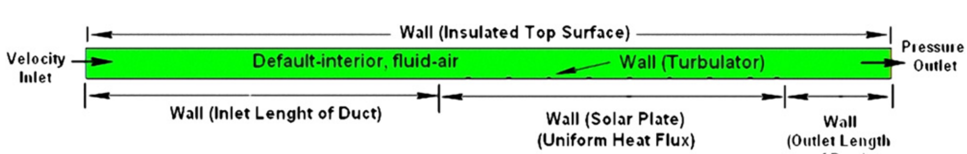


Fig. 13. Boundary condition of solution domain.

the redevelopment of two boundary layers at the reattachment point in between two adjacent ribs. (2) Roughness pitch strongly affected the flow pattern and also performance of the duct. The turbulator geometry showed appreciable heat transfer even at low Reynolds number ($Re<5000$) where rib effect was inefficient. (3) Value of the Nusselt number increased sharply at high Reynolds number and this became constant or increased very slightly at low Reynolds number. (4) In the inter-rib region, the model predicted well near the central high heat transfer area but it under predicted around ribs. (5) Peaks of local heat transfer were found at the reattachment points. Experiments also confirmed it. (6) Turbulence intensity was found maximum at peak of the local heat transfer coefficient in the inter-rib regions. (7) The turbulences generated only in the viscous sub-layer region of boundary layer resulted in better thermo-hydraulic performance i.e., maximum heat transfer at affordable friction penalty. (8) Results obtained by Renormalization-group (RNG) k–ε model were in good agreement with the available experimental data.

Sharma et al. [59] designed a solar air heater duct in accordance with the guidelines given in ASHARE standard [1977] in order to carry out CFD based investigation. CFD based performance analysis of solar air heater duct provided with artificial roughness in the form of square type protrusion shape geometry was reported. 2D computational domain and grid were selected. Non-uniform meshing was generated over the duct. Following conclusions were drawn from this CFD simulation: (1) with the application of such type of artificial roughness, heat transfer coefficient enhanced at the cost of frictional penalty. (2) Nusselt number and friction factor correlations were developed by using CFD data. (3) For a given value of relative roughness pitch (p/e) Nusselt number increased with an increase of Reynolds number. Nusselt number was found maximum at minimum value of relative roughness pitch (p/e). (4) For a given value of relative roughness pitch (p/e) the friction factor decreased with increase of Reynolds number. (5) An Average absolute percentage deviation between CFD and predicted data of Nusselt number and friction factor was found $\pm$15%.

Sharma and Thakur [60] conducted a CFD study to investigate the heat transfer and friction loss characteristics in a solar air heater having attachments of V-shaped ribs roughness at 60° relative to flow direction pointing downstream on underside of the absorber plate. The computations based on the finite volume method with the SIMPLE algorithm were conducted for the air flow in terms of Reynolds numbers ranging from 5000 to 15,000. Fig. 14 shows the computational domain used for CFD analysis. Figs. 15 and 16 show the contour of heat flux on the roughened duct and temperature contour of rib roughened plate in three dimensions obtained from CFD analysis respectively. Following conclusions were drawn from this CFD simulation: (1) Combined effect of swirling motion, detachment and reattachment of fluid were responsible in the increase of heat transfer rate during CFD analysis. (2) Nusselt number increased with increase in Reynolds number whereas friction factor decreased with increase in Reynolds number for all combinations of relative

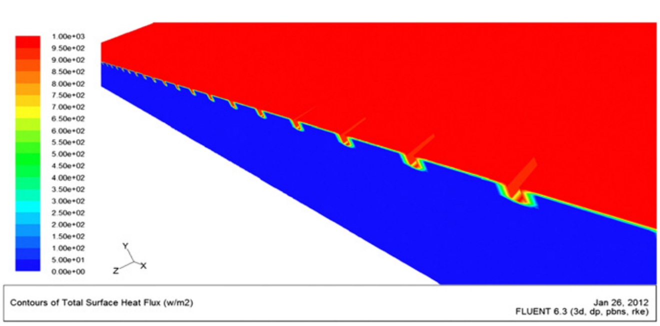


Fig. 15. Contour plot of heat flux on the roughened duct.

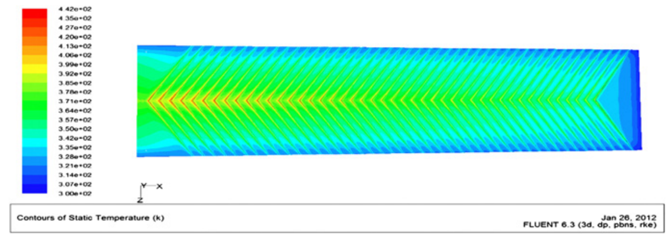


Fig. 16. Temperature contour of rib roughened plate.

roughness height (e/D) and relative roughness pitch (P/e). (3) For validating the accuracy of numerical solutions, the computations of fully developed turbulent flow forced convection in a smooth rectangular duct was carried out to compare with the exact solution for Nusselt number and friction factor, respectively. The present numerical smooth channel results were found to be in excellent agreement with the exact solutions obtained from the literature. An average absolute percentage deviation between CFD and predicted data of Nusselt number and friction factor was found less than $\pm$3%. (4) The v shaped rib roughness gave high rate of heat transfer.

Gandhi and Singh [61] conducted a CFD study to investigate the effect of artificial surface roughness on flow through a rectangular duct having bottom wall roughened with repeated transverse ribs of wedge shaped cross-section. CFD investigations were carried out for a range of Reynolds number from 5000 to 21,000 for a smooth duct and a roughened duct of relative roughness height of 0.022, relative roughness pitch of 4.5 and rib wedge angle of 15°. Numerical results obtained by commercial computational fluid dynamics (CFD) code FLUENT were compared with the experimental results. Two dimensional numerical modeling of the duct flow using FLUENT showed reasonably good agreement with the experimental observations except for the friction factor. Following conclusions were drawn: (1) Rib-roughened surface in a rectangular duct produced much flatter velocity profile and higher turbulence intensities as compared to the smooth surface. This enhanced the heat transfer in case of the roughened duct. (2) CFD analysis of the velocity profile and turbulence intensity was found reasonably well with the experimental results for k–ε turbulence model. (3) Friction factor for roughened duct was around 3.4 times higher than the smooth duct at Reynolds number of 21,000.

This review of literature reveals that very few studies have been done on prediction of heat transfer and fluid flow in solar air heater using CFD (Table 2). CFD modeling was originally developed for industrial application. Today it is being used widely in research work, product development, and in almost all sphere of activity where a detailed picture of phenomena involving heat transfer and fluid flow, phase change etc. is desired. Presently CFD techniques are increasingly used to model flow through solar air heater. The advantages of computational simulations are that they can produce extremely large volumes of results at virtually no added expense and it is very cheap to perform parametric studies to optimize equipment performance. The second reason for such work on computational simulation is that some parameters are difficult to test, and experimental study is expensive as well as time consuming. The results obtained with the CFD are of acceptable quality.

5. Discussion about turbulence models

The literature survey reveals that the solar air heaters are thermo-hydraulically more efficient if system operates at Reynolds numbers ranges from 3000 to 19,000. Reynolds number inside the rectangular duct of solar air heater shows that the flow is turbulent. One of the great challenges in the

Table 2
CFD simulations of solar air heater.

Authors	Computational methodology	Difference between experimental and simulation results
Arulanandam et al. [48]	• CFD code: TASC flow • Turbulence model: – • Mesh: uniform	Close agreement observed
Ammari [49]	Fortran	Good agreement observed
Chaube et al. [50]	• CFD code: Fluent 6.1 • Turbulence model: SST $k–\omega$ • Mesh: rectangular, non-uniform	Good agreement observed
Chaube et al. [51]	• CFD code: Fluent 6.1 • Turbulence model: SST $k–\omega$ • Mesh: rectangular, non-uniform	Good agreement observed
Wang et al. [52]	–	Good agreement observed
Varol and Oztop [53]	• CFD code: CFDRC ACE+ • Turbulence model: – • Mesh: Non-uniform	Good agreement observed
Kumar and Saini [54]	• CFD Code: Fluent 6.3.26 • Turbulence model: RNG $k–\varepsilon$ • Mesh: non-uniform	Good agreement observed
Karmare and Tikekar [55]	• CFD code: Fluent 6.2.16 • Turbulence model: RNG $k–\varepsilon$ • Mesh: non-uniform	Good agreement observed
Soi et al. [56]	• CFD code: Fluent • Turbulence model: RNG $k–\varepsilon$ • Mesh: non-uniform	Nusselt number $\pm 15\%$ Friction factor $\pm 20\%$
Giri [57]	• CFD code: Fluent • Turbulence Model: RNG $k–\varepsilon$ • Mesh: Non-uniform	Good agreement observed
Rajput [58]	• CFD code: Fluent • Turbulent model: RNG $k–\varepsilon$ • Mesh: uniform	Good agreement observed
Sharma et al. [59]	• CFD code: Fluent • Turbulence model: RNG $k–\varepsilon$ • Mesh: non-uniform	Nusselt number $\pm 15\%$ Friction factor $\pm 15\%$
Sharma and Thakur [60]	• CFD code: Fluent • Turbulent model: Realizable $k–\varepsilon$ • Mesh: uniform	Nusselt number $\pm 3\%$ Friction factor $\pm 3\%$
Gandhi and Singh [61]	• CFD code: Fluent • Turbulence model: $k–\omega$ • Mesh: Uniform	Good agreement observed except for the friction factor

design of a solar air heater using CFD approach is the selection of appropriate turbulence model. When CFD simulations of a flow through a solar air heater are concerned, we often wonder, whether the simulation produces a precise image of the real flow. The question is not answered easily, as the quality of the obtained result depends on many parameters of the computer model. Modern CFD programs offer their users many possible parameters of the mathematical model. However, if various turbulence models are available, the user may wonder which of them is the best suited for a solar air heater system. The authors attempt to answer this question in the present article.

A turbulence model is a computational procedure to close the system of mean flow equations. Turbulence models allow the calculation of the mean flow without first calculating the full time-dependent flow field. Modern CFD programs offer a large range of methods and models to simulate turbulence. The methods include [62]:

1. Reynolds-average simulation (RAS)/Reynolds-averaged Navier–Stokes (RANS): The governing equations are solved in ensemble-averaged form, including appropriate models for the effect of turbulence. Different types of incompressible and compressible RANS models are listed in Table 3.
2. Large eddy simulation (LES): Large turbulent structures in the flow are resolved by the governing equations, while the effect of the sub-grid scales (SGS) are modeled. The scale separation is obtained by applying a filter to the governing equations which also influences the form of the SGS models. Different types of LES models are listed in Table 4.
3. Detached eddy simulation (DES): Hybrid method that treats near-wall regions with a RAS approach and the bulk flow with

Table 3
RAS turbulence models.

RAS turbulence models for incompressible fluids	
laminar	Dummy turbulence model for laminar flow
kEpsilon	Standard high-*Re* k–ε model
kOmega	Standard high-*Re* k–ω model
kOmegaSST	k–ω-SST model
RNGkEpsilon	RNG k–ε model
NonlinearKEShih	Non-linear Shih k–ε model
LienCubicKE	Lien cubic k–ε model
qZeta	q–ς model
LaunderSharmaKE	Launder–Sharma low-*Re* k–ε model
LamBremhorstKE	Lam–Bremhorst low-*Re* k–ε model
LienCubicKELowRe	Lien cubic low-*Re* k–ε model
LienLeschzinerLowRe	Lien-Leschziner low-*Re* k–ε model
LRR	Launder–Reece–Rodi RSTM
LaunderGibsonRSTM	Launder–Gibson RSTM with wall-reflection terms
realizableKE	Realizable k–ε model
SpalartAllmaras	Spalart–Allmaras 1-eqn mixing-length model
RAS turbulence models for compressible fluids	
laminar	Dummy turbulence model for laminar flow
kEpsilon	Standard k–ε model
kOmegaSST	k–ω-SST model
RNGkEpsilon	RNG k–ε model
LaunderSharmaKE	Launder–Sharma low-*Re* k–ε model
LRR	Launder–Reece–Rodi RSTM
LaunderGibsonRSTM	Launder–Gibson RSTM
realizableKE	Realizable k–ε model
SpalartAllmaras	Spalart–Allmaras 1-eqn mixing-length model

Table 4
LES turbulence models.

Isochoric LES turbulence models	
Smagorinsky	Smagorinsky model
Smagorinsky2	Smagorinsky model with 3D filter
dynSmagorinsky	Dynamic Smagorinsky
homogenousDynSmagorinsky	Homogeneous dynamic Smagorinsky model
dynLagrangian	Lagrangian two equation eddy-viscosity model
scaleSimilarity	Scale similarity model
mixedSmagorinsky	Mixed Smagorinsky/scale similarity model
dynMixedSmagorinsky	Dynamic mixed Smagorinsky/scale similarity model
kOmegaSSTSAS	k–ω-SST scale adaptive simulation (SAS) model
oneEqEddy	k-equation eddy-viscosity model
dynOneEqEddy	Dynamic k-equation eddy-viscosity model
locDynOneEqEddy	Localised dynamic k-equation eddy-viscosity model
spectEddyVisc	Spectral eddy viscosity model
LRRDiffStress	LRR differential stress model
DeardorffDiffStress	Deardorff differential stress model
SpalartAllmaras	Spalart–Allmaras model
SpalartAllmarasDDES	Spalart–Allmaras delayed detached eddy simulation (DDES) model
SpalartAllmarasIDDES	Spalart–Allmaras improved DDES (IDDES) model
Anisochoric LES turbulence models	
Smagorinsky	Smagorinsky model
oneEqEddy	k-equation eddy-viscosity model
dynOneEqEddy	Dynamic k-equation eddy-viscosity model
lowReOneEqEddy	Low-*Re* k-equation eddy-viscosity model
DeardorffDiffStress	Deardorff differential stress model
SpalartAllmaras	Spalart–Allmaras 1-eqn mixing-length model
LES deltas	
PrandtlDelta	Prandtl delta
cubeRootVolDelta	Cube root of cell volume delta
maxDeltaxyz	Maximum of x, y and z; for structured hex cells only
smoothDelta	Smoothing of delta
LES filters	
laplaceFilter	Laplace filters
simpleFilter	Simple filter
anisotropicFilter	Anisotropic filter

an LES approach. Table 4 also includes detached eddy simulation (DES) models.

4. Direct numerical simulation (DNS): Resolves all scales of turbulence by solving the Navier–Stokes equations numerically without any turbulence modeling.

A number of software based on CFD codes have been developed, few of them are: CFX, FLUENT, PHOENICS, FLOVENT and STAR-CD. Each software is usually supported by supplementary software for different applications, such as domain model preparation, mesh generation etc. Under the present study, commercial CFD code ANSYS FLUENT v12.1 is used. There are several turbulence model included in the commercial CFD software ANSYS FLUENT v12.1. The following turbulence models, available in ANSYS FLUENT v12.1, are tested: Standard k–ε turbulence model, Realizable k–ε turbulence model, Renormalization-group (RNG) k–ε turbulence model, Standard k–ω turbulence model, and Shear Stress Transport (SST) k–ω turbulence model.

6. Selection of best turbulence model

In this section a 2-dimentional CFD simulation of investigated in order to find out the best turbulence model for the analysis of a solar air heater. Commercial CFD simulation code FLUENT (version 12.1) is used as a solver. The following assumptions are imposed for the computational analysis.

1. The flow is steady, fully developed, turbulent and two dimensional.
2. The thermal conductivity of the duct wall, absorber plate and roughness material are independent of temperature.
3. The duct wall and absorber plate are homogeneous and isotropic.
4. No-slip boundary condition is assigned to the walls in contact with the fluid in the model.
5. Negligible radiation heat transfer and other heat losses.

The 2D computational domain used for CFD analysis having the height of 20 mm, width of 200 mm and length of 461 mm. Fig. 17 shows the 2D computational domain used in this study. Complete duct geometry is divided into three sections, namely, entrance section, test section and exit section. A short entrance length is chosen because for a roughened duct, the thermally fully developed flow is established in a short length 2–3 times hydraulic diameter. The exit section is used after the test section in order to reduce the end effect in the test section. For the turbulent flow regime, ASHRAE Standard 93-2003 recommends entrance and exit length of $5\sqrt{WH}$ and $2.5\sqrt{WH}$, respectively [63]. The top wall consists of a 0.5 mm thick absorber plate made up of aluminum. A uniform heat flux of 1000 W/m^2 is considered for computational analysis. The geometrical and operating parameters employed in this computational investigation are listed in Table 5.

The flow phenomenon in a conventional solar air heater duct is governed by the continuity, momentum and energy equations. In the Cartesian tensor system these equations can be written as:

Continuity equation:

$$\frac{\partial}{\partial x_i}(\rho u_i) = 0 \tag{9}$$

Momentum equation:

$$\frac{\partial}{\partial x_i}(\rho u_i u_j) = -\frac{\partial p}{\partial x_i} + \frac{\partial}{\partial x_j}\left[\mu\left(\frac{\partial u_i}{\partial x_j} + \frac{\partial u_j}{\partial x_i}\right)\right] + \frac{\partial}{\partial x_j}(-\rho\overline{u_i' u_j'}) \tag{10}$$

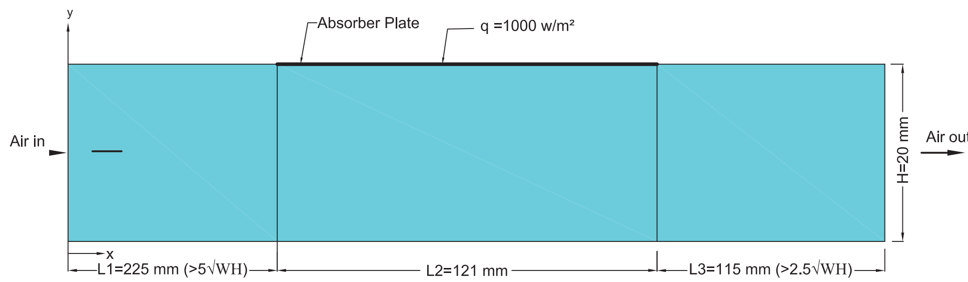


Fig. 17. Schematic of two-dimensional solution domain for CFD analysis

Table 5
Geometrical and operating parameters for computational analysis.

Geometrical and operating parameters	Range
Entrance length of duct, 'L_1'	225 mm
Test length of duct, 'L_2'	115 mm
Exit length of duct, 'L_3'	121 mm
Width of duct, '*W*'	100 mm
Depth of duct, '*H*'	20 mm
Hydraulic diameter of duct, '*D*'	33.33 mm
Duct aspect ratio, '*W/H*'	5
Uniform heat flux, '*I*'	1,000 W/m^2
Reynolds number, '*Re*'	3,800–18,000 (6 values)
Prandtl number, '*Pr*'	0.7441

Table 6
Thermo-physical properties of working fluid (air) and absorber plate (aluminum) for computational analysis.

Properties	Working fluid (air)	Absorber plate (aluminum)
Density, 'ρ' (kg/m^3)	1.225	2719
Specific heat, 'C_p' (J/kg//K)	1006.43	871
Viscosity, 'μ' (N/m^2)	1.7894e − 05	–
Thermal conductivity, '*k*'(W/m//K)	0.0242	202.4

Energy equation:

$$\frac{\partial}{\partial x_i}(\rho u_i T) = \frac{\partial}{\partial x_j}\left((\Gamma + \Gamma_t)\frac{\partial T}{\partial x_j}\right) \quad (11)$$

where Γ and Γ_t are molecular thermal diffusivity and turbulent thermal diffusivity, respectively, and are given by

$$\Gamma = \mu/Pr \quad \text{and} \quad \Gamma_t = \mu_t/Pr_t \quad (12)$$

The following boundary conditions are assigned in FLUENT:

1. Velocity at inlet (depending on Reynolds number)
2. Turbulence intensity at inlet (depending on Reynolds number)
3. Hydraulic diameter of duct (fixed)
4. Pressure at outlet (fixed atmospheric pressure)
5. Constant heat flux on broad bottom surface of test section
6. No heat transfer from other walls of the duct.

The properties of the working fluid (air) and absorber plate material (aluminum) are assumed to remain constant at average bulk temperature. The thermo-physical properties of working fluid and absorber plate are illustrated in Table 6.

Meshing of the domain is generated using ANSYS ICEM CFD V12.1 software. A uniform mesh with very fine mesh size near the wall is used to resolve the laminar sub-layer as shown in Fig. 18. Present uniform quadrilateral mesh contains 45,951 nodes and 45,000 cells. An exponential function is used to concentrate the fine mesh near the wall to reserve the high-velocity gradients near the walls. The first grid point from the wall is carefully adjusted to be located in the linear region to ensure that non-dimensional wall distance y^+ is less than 1.0.

In the present simulation governing equations of continuity, momentum and energy are solved by the finite volume method in the steady-state regime using the commercial CFD code ANSYS FLUENT v12.1. A second-order upwind scheme is chosen for energy and momentum equations. The SIMPLE algorithm (semi-implicit method for pressure linked equations) is chosen as scheme to couple pressure and velocity [64]. A uniform air velocity is introduced at the inlet while a constant pressure outlet

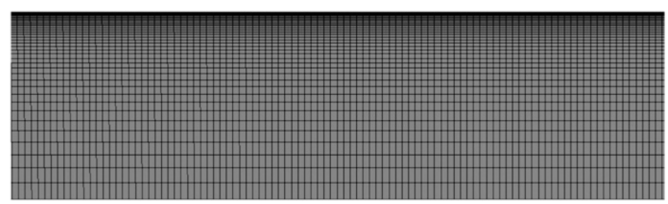


Fig. 18. Close up view of the two-dimensional structured mesh.

condition is applied at the outlet. Adiabatic boundary condition is implemented over the bottom duct wall while constant heat flux condition is applied to the upper duct wall of test section. After completing all the relevant settings FLUENT starts to perform the calculation in an iterative manner until a sufficient tolerance, defined by the user, is achieved. The convergence criteria of 10^{-6} for the residuals of the continuity equation, 10^{-3} for the residuals of the velocity components and 10^{-6} for the residuals of the energy are assumed.

To achieve the accurate prediction of heat transfer and friction factor in a solar air heater, the predictive ability of five different turbulence models including: The Standard k–ε turbulence model, the Realizable k–ε turbulence model, the Renormalization-group (RNG) k–ε turbulence model, the Standard k–ω turbulence model, and the Shear Stress Transport (SST) k–ω turbulence model, are investigated and compared with the available experimental data.

Fig. 19 shows the variation of average Nusselt number with Reynolds number for different turbulence models and empirical correlation available for conventional solar air heater i.e., Dittus–Boelter correlation [65].

$$\text{Dittus}-\text{Boelter equation}: Nu = 0.023Re^{0.8}Pr^{0.4} \quad (13)$$

The average Nusselt number is observed to increase with increase in Reynolds number for all turbulence models. It is observed that the results obtained by Renormalization-group (RNG) k–ε model are in good agreement with the Dittus–Boelter empirical correlation results. The average absolute percentage deviations between the values predicted by Standard k–ω model and Dittus–Boelter empirical correlation results is found to be $\pm 3.58\%$ for Nusselt number. Prediction by Standard k–ω model shows more deviation with Dittus–Boelter empirical correlation results.

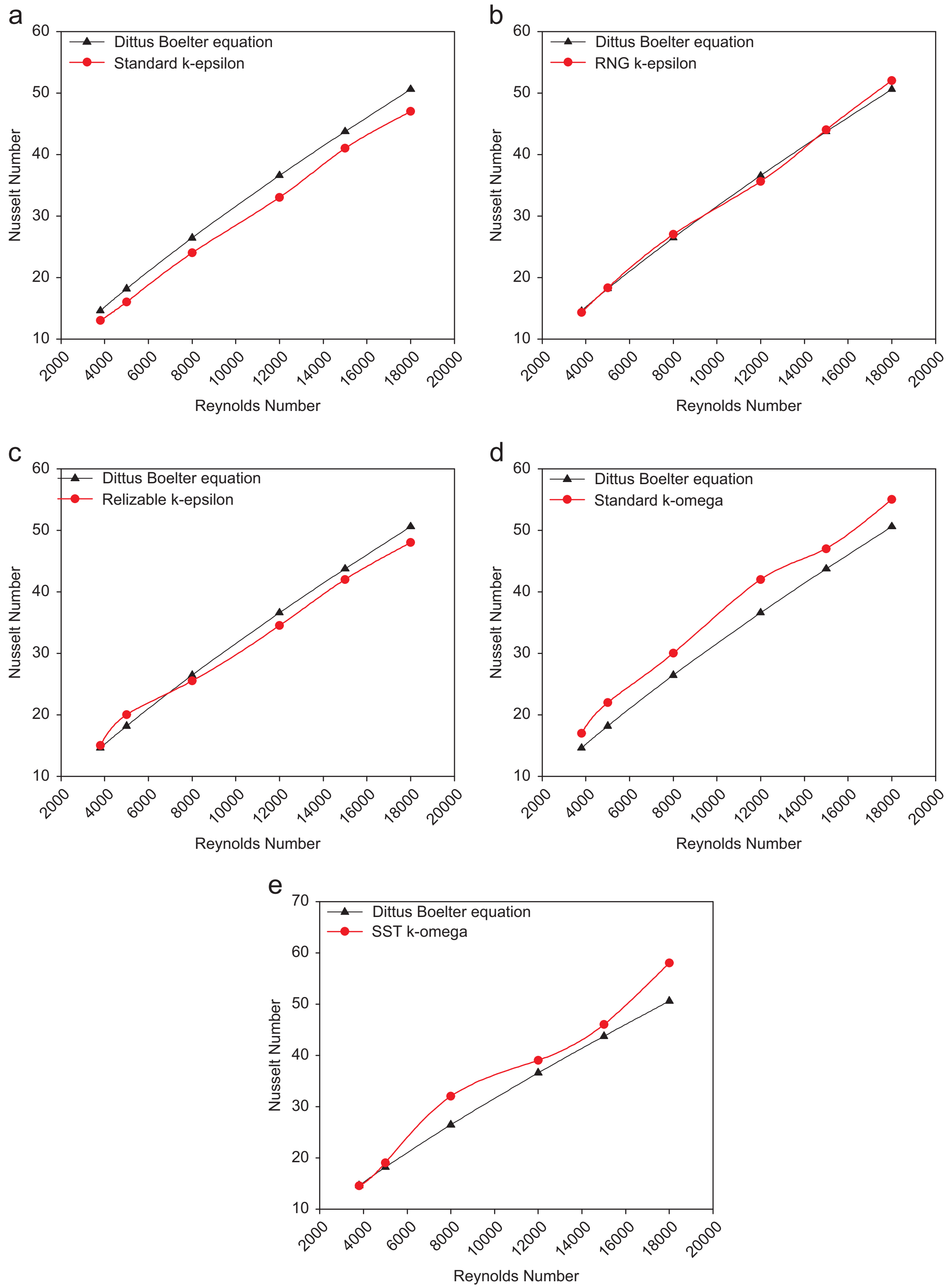


Fig. 19. Variation of Nusselt number with Reynolds number using (a) Standard k–ε turbulence model, (b) RNG k–ε turbulence model, (c) Realizable k–ε turbulence model, (d) Standard k–ω turbulence model and (e) SST k–ω turbulence model.

The predictions with the Standard k–ω model and the SST k–ω model are over-predicted in comparison with Dittus–Boelter empirical correlation results whereas Standard k–ε model and Realizable k–ε model are under-predicted.

Fig. 20 shows the variation of average friction factor with Reynolds number for different turbulence models and empirical correlation available for conventional solar air heater i.e., Blasius correlation [66].

$$\text{Blasius equation}: f = 0.0791Re^{-0.25} \quad (14)$$

It is also observed that the results obtained by Renormalization-group (RNG) k–ε model are in good agreement with the Blasius equation empirical correlation results. The average absolute percentage deviations between the values predicted by Standard k–ω

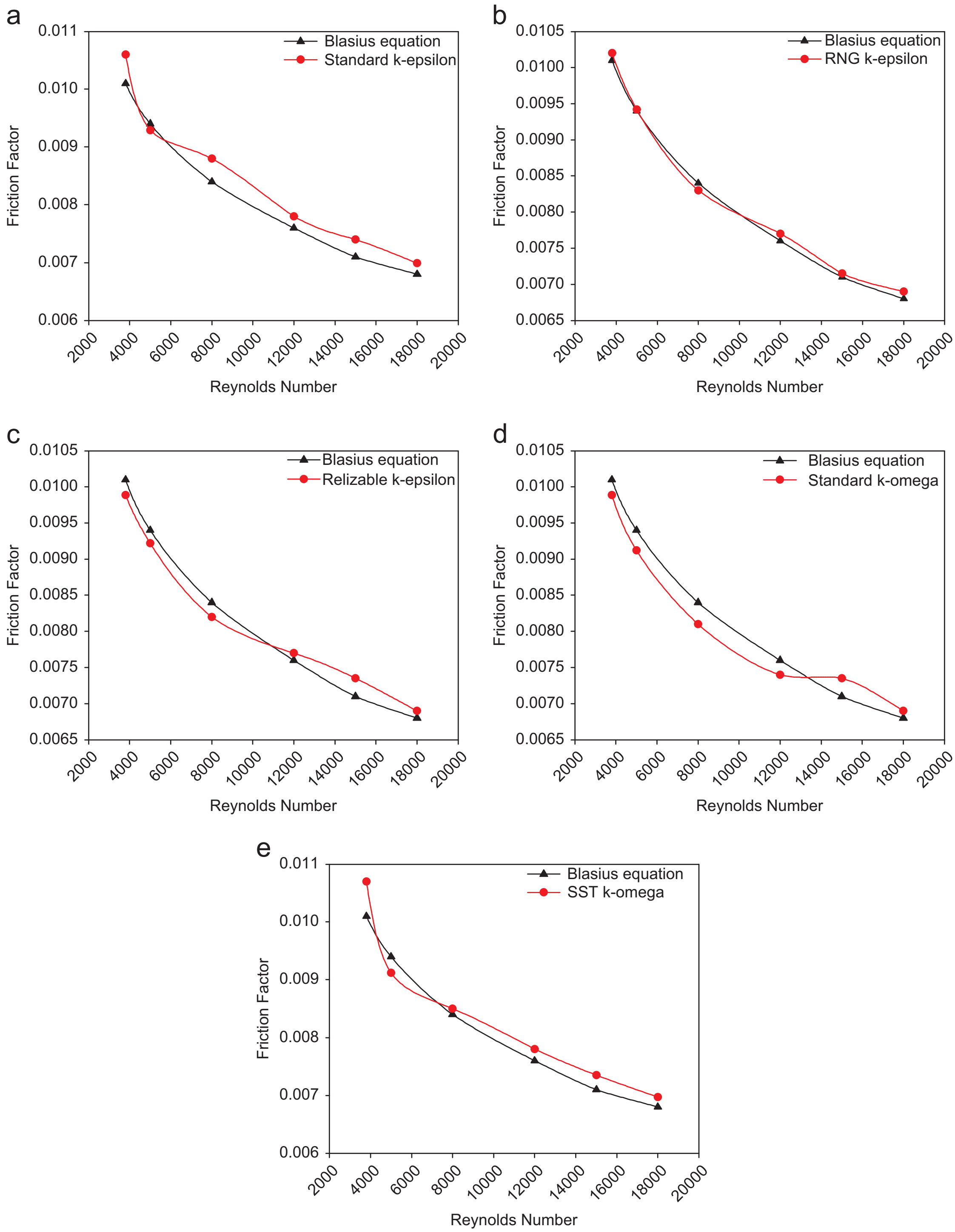


Fig. 20. Variation of friction factor with Reynolds number using (a) Standard k–ε turbulence model, (b) RNG k–ε turbulence model, (c) Realizable k–ε turbulence model, (d) Standard k–ω turbulence model and (e) SST k–ω turbulence model.

model and Blasius empirical correlation results is found to be $\pm$3.28% for friction factor. Prediction by Standard k–ω model shows more deviation with Blasius empirical correlation results.

Five different turbulence models, for steady state conditions, available in FLUENT, are tested and the RNG k–ε model is proven as the most appropriate. The computed average Nusselt number and friction factor are in very good agreement with the corresponding experimental values.

Finally, it can be concluded that the Renormalization-group (RNG) k–ε turbulence model predicts very close results to the experimental results, which yields confidence in the predictions done by CFD analysis in the design of a solar air heater.

7. Conclusions

This article presents a detailed review of the literature that deals with the application of CFD in design of solar air heater. In this article a CFD investigation is also carried out to select best turbulence model for the design of a solar air heater. A modern

CFD code ANSYS FLUENT v12.1 is used to simulate fluid flow through a conventional solar air heater. A two-dimensional flow is assumed. The influences of the five different turbulence models on the quality of the obtained results are tested. On the basis of the review of the literature and CFD investigation of solar air heater, the conclusion can be summarized as follows:

1. This review of literature reveals that a lot of work has been reported on design of solar air heater by experimental approach. This review also reveals that a few studies have been done on CFD analysis of solar air heater.
2. CFD simulation results are found to be in good agreement with experimental results and with the standard theoretical approaches. Although there are some small discrepancies due to some experimental imperfectness matters, we still have a good confidence in the CFD simulation program that can be used in the future for more complex solar air heater problem.
3. There is no doubt that a major focus of CFD analysis of solar air heater is to enhance the design process that deals with the heat transfer and fluid flow.
4. In recent years CFD has been applied in the design of solar air heater. The quality of the solutions obtained from CFD simulations are largely within the acceptable range proving that CFD is an effective tool for predicting the behaviour and performance of a solar air heater.
5. One of the great challenges in the design of a solar air heater using CFD approach is the selection of appropriate turbulence model. The decision about a suitable turbulence model chosen in a CFD computation is not easy.
6. The influences of the five different turbulence models such as: Standard k–ε turbulence model, the Realizable k–ε turbulence model, the Renormalization-group (RNG) k–ε turbulence model, the Standard k–ω turbulence model, and the Shear Stress Transport (SST) k–ω turbulence model on the quality of the obtained results are tested. It appears from the performed calculations that the Renormalization-group k–ε model yields the best results for two-dimensional flows through a conventional solar air heater.

In summary, the purpose of this article is to illustrate the modern use of CFD in design of solar air heater and to use this to indicate the wide-open future of CFD design. No matter how mature the techniques of CFD may become, the array of future and challenging applications of CFD is limitless. There is tremendous scope for future study of solar air heater with CFD approach. The information presented here will be beneficial for beginners in this area of research. Authors hope that this article has opened the horizons of CFD analysis of solar air heater to researchers.

References

[1] Foster R, Ghassemi M, Cota A. Solar energy: renewable energy and the environment. New York: CRC Press Taylor & Francis group; 2010.
[2] Li X. Green energy: basic concepts and fundamentals. 1st ed.. New York: Springer; 2011.
[3] Maczulak A. Renewable energy: sources and methods. 1st ed.. New York: Infobase Publishing; 2011.
[4] Kaltschmitt M, Streicher W, Wiese A. Renewable energy: technology, economics and environment. 1st ed.. New York: Springer; 2007.
[5] Quaschning V. Understanding renewable energy systems. 3rd ed.. London: Earthscan; 2005.
[6] Twidell J, Weir T. Renewable energy: sources. 2nd ed.. New York: Taylor & Francis; 2006.
[7] Sukhatme SP, Nayak JP. Solar energy. 3rd ed.. New Delhi: Tata McGraw Hill; 2011.
[8] Date AW. Introduction to computational fluid dynamics. 1st ed.. New York: Cambridge University Press; 2005.
[9] Chung TJ, editor. Cambridge UK: Cambridge University Press; 2002.
[10] Cebeci T, Kafyeke F, Shao JP, Laurendeau E. Computational fluid dynamics for engineers. 1st ed.. New York: Springer; 2005.
[11] Ferziger JH, Peric M. Computational method for fluid dynamics. 3rd ed.. New York: Springer; 2002.
[12] Andreson Jr JD. Computational fluid dynamics—the basics with applications. 1st ed.. New York: Mcgraw-Hill; 1995.
[13] Blazek J. Computational fluid dynamics—principles and applications. 1st ed.. Oxford, UK: Elsevier; 2001.
[14] Garg HP, Prakash J. Solar energy fundamentals and applications. 1st ed.. New Delhi: Tata McGraw-Hill; 2000.
[15] Duffie JA, Beckman WA. Solar engineering of thermal processes. 2nd ed.. New York: Wiley; 1980.
[16] Patankar SV. Numerical heat transfer and fluid flow. 1st ed.. USA: Hemisphere Publishing Corporation; 1980.
[17] Tannehill JC, Andeson DA, Pletcher RH. Computational fluid mechanics and heat transfer. 2nd ed.. London: Taylor & Francis; 1997.
[18] Versteeg HK, Malalasekera W. An introduction to computational fluid dynamics. 2nd ed.. England: Pearson Education Limited; 2007.
[19] Kumar A, Bhagoria JL, Sarviya RM. Heat transfer and friction correlations for artificially roughened solar air heater duct with discrete W-shaped ribs. Energy Conversion and Management 2009;50:2106–17.
[20] Mittal MK, Varun RP, Singal SK. Effective efficiency of solar air heaters having different types of roughness elements on absorber plate. Energy 2007;32:739–45.
[21] Prasad BN, Saini JS. Optimal thermohydraulic performance of artificially roughened solar air heaters. Solar Energy 1991;47(2):91–6.
[22] Prasad BN, Saini JS. Effect of artificial roughness on heat transfer and friction factor in a solar air heater. Solar Energy 1988;41(6):555–60.
[23] Aharwal KR, Gandhi BK, Saini JS. Experimental investigation on heat-transfer enhancement to a gap in an inclined continuous rib arrangement in a rectangular duct of solar air heater. Renew Energy 2008;33:585–96.
[24] Muluwork KB. Investigations on fluid flow and heat transfer in roughened absorber solar heaters. PhD thesis. IIT Roorkee, India; 2000.
[25] Prasad K, Mullick SC. Heat transfer characteristics of a solar air heater used for drying purposes. Applied Energy 1983;13:83–93.
[26] Gupta D, Solanki SC, Saini JS. Heat and fluid flow in rectangular solar air heater ducts having transverse rib roughness on absorber plates. Solar Energy 1993;51(1):31–7.
[27] Verma SK, Prasad BN. Investigation for the optimal thermohydraulic performance of artificially roughened solar air heaters. Renewal Energy 2000;20(1):19–36.
[28] Karwa R. Experimental studies of augmented heat transfer and friction in asymmetrically heated rectangular ducts with ribs on heated wall in transverse, inclined, v-continuous and v- discrete pattern. International Communications in Heat and Mass Transfer 2003;30(2):241–50.
[29] Sahu MM, Bhagoria JL. Augmentation of heat transfer coefficient by using 90° broken transverse ribs on absorber plate of solar air heater. Renewable Energy 2005;30:2057–73.
[30] Gupta D, Solanki SC, Saini JS. Thermohydraulic performance of solar air heaters with roughened absorber plates. Solar Energy 1997;61(1):33–42.
[31] Saini RP, Saini JS. Heat transfer and friction factor correlations for artificially roughened ducts with expanded metal mesh as roughened element. International Communications in Heat and Mass Transfer 1997;40(4):973–86.
[32] Momin AME, Saini JS, Solanki SC. Heat transfer and friction in solar air heater duct with v- shaped rib roughness on absorber plate. International Communications in Heat and Mass Transfer 2002;45:3383–96.
[33] Karwa R, Bairwa RD, Jain BP, Karwa N. Experimental study of the effects of rib angle and discretization on heat transfer and friction in an asymmetrically heated rectangular duct. Journal of Enhanced Heat Transfer 2005;12(4):343–55.
[34] Karwa R, Solanki SC, Saini JS. Heat transfer coefficient and friction factor correlations for the transitional flow regime in rib-roughened rectangular ducts. International Communications in Heat and Mass Transfer 1999;42:1597–615.
[35] Bhagoria JL, Saini JS, Solanki SC. Heat transfer coefficient and friction factor correlations for rectangular solar air heater duct having transverse wedge shaped rib roughness on the absorber plate. Renewal Energy 2002;25:341–69.
[36] Saini SK, Saini RP. Development of correlations for Nusselt number and friction factor for solar air heater with roughened duct having arc-shaped wire as artificial roughness. Solar Energy 2008;82:1118–30.
[37] Saini RP, Verma J. Heat transfer and friction factor correlations for a duct having dimple- shaped artificial roughness for solar air heaters. Energy 2008;33:1277–87.
[38] Karmare SV, Tikekar AN. Heat transfer and friction factor correlation for artificially roughened duct with metal grit ribs. International Journal of Heat and Mass Transfer 2007;50:4342–51.
[39] Kumar A, Bhagoria JL, Sarviya RM. Heat transfer enhancement in channel of solar air collector by using discrete W-shaped artificial roughened absorber. In: 19th National & 8th ISHMT-ASME heat and mass transfer conference; 2008.
[40] Jaurker AR, Saini JS, Gandhi BK. Heat transfer and friction characteristics of rectangular solar air heater duct using rib-grooved artificial roughness. Solar Energy 2006;80:895–907.
[41] Layek A, Saini JS, Solanki SC. Second law optimization of a solar air heater having chamfered rib-groove roughness on absorber plate. Renewable Energy 2007;32(12):1967–80.
[42] Varun RP, Singal SK. Investigation of thermal performance of solar air heater having roughness elements as a combination of inclined and transverse ribs on absorber plate. Renewable Energy 2008;33:1398–405.

[43] Lanjewar A, Bhagoria JL, Sarviya RM. Heat transfer and friction in solar air heater duct with W-shaped rib roughness on absorber plate. Energy 2011;36:4531–41.
[44] Varun RP, Singal SK. A review on roughness geometry used in solar air heaters. Solar Energy 2007;81:1340–50.
[45] Hans VS, Saini RP, Saini JS. Performance of artificially roughened solar air heaters- A review. Renewable and Sustainable Energy Reviews 2009;13: 1854–69.
[46] Bhushan B, Singh R. A review on methodology of artificial roughness used in duct of solar air heaters. Energy 2010;35:202–12.
[47] Kumar A, Saini RP, Saini JS. Heat and fluid flow characteristics of roughened solar air heater ducts—a review. Renewable Energy 2012;47:77–94.
[48] Arulanandam SJ, Hollands KGT, Brundrett E. A CFD heat transfer analysis of the transpired solar collector under no-wind conditions. Solar Energy 1999;67(1–3):93–100.
[49] Ammari HD. A mathematical model of thermal performance of a solar air heater with slats. Renewable Energy 2003;28:1597–615.
[50] Chaube A, Sahoo PK, Solanki SC. Analysis of heat transfer augmentation and flow characteristics due to rib roughness over absorber plate of a solar air heater. Renewable Energy 2006;31:317–31.
[51] Chaube A, Sahoo PK, Solanki SC. Effect of roughness shape on heat transfer and flow friction characteristics of solar air heater with roughened absorber plate. WIT Transactions on Engineering Sciences 2006;53:43–51.
[52] Wang C, Guan Z, Zhao X, Wang D. Numerical simulation study on transpired solar air collector. In: Proceedings of the sixth international conference for enhanced building operations, 6–9 November 2006, Shenzhen, China; 2006.
[53] Varol Y, Oztop HF. A comparative numerical study on natural convection in inclined wavy and flat-plate solar collectors. Building and Environment 2008;43:1535–44.
[54] Kumar S, Saini RP. CFD based performance analysis of a solar air heater duct provided with artificial roughness. Renewable Energy 2009;34:1285–91.
[55] Karmare SV, Tikekar AN. Analysis of fluid flow and heat transfer in a rib grit roughened surface solar air heater using CFD. Solar Energy 2010;84:409–17.
[56] Soi A, Singh R, Bhushan B. Effect of roughness element pitch on heat transfer and friction characteristics of artificially roughened solar air heater duct. International Journal of Advanced Engineering Technology 2010;1(3): 339–46.
[57] Giri AK. CFD analysis of reattachment point, heat transfer and fluid flow of a solar air heater duct provided with artificial roughness. M.Tech. dissertation. MANIT Bhopal, India; 2010.
[58] Rajput RS. Heat transfer and fluid flow analysis of inverted U-type turbulator in a solar air heater duct by CFD. M.Tech. dissertation. MANIT Bhopal, India; 2010.
[59] Sharma S, Singh R, Bhushan B. CFD based investigation on effect of roughness element pitch on performance of artificially roughened duct used in solar air heaters. International Journal of Advanced Engineering Technology 2011;2(1): 234–41.
[60] Sharma AK, Thakur NS. CFD based fluid flow and heat transfer analysis of a v- shaped roughened surface solar air heater. International Journal of Advanced Engineering Technology 2012;4(5):2115–21.
[61] Gandhi BK, Singh KM. Experimental and numerical investigations on flow through wedge shape rib roughened duct. The Institution of Engineers (India) Journal—MC 2010;90:13–8 January.
[62] OpenFOAM, Internet: 〈www.openfoam.com/features/turbulence.php〉; [accessed 08.02.13].
[63] ASHRAE Standard 93. Method of testing to determine the thermal performance of solar collectors. American Society of Heating, Refrigeration and Air Conditioning Engineers, Atlanta, GA30329; 2003.
[64] Patankar SV. Numerical heat transfer and fluid flow. Washington DC: Hemisphere; 1980.
[65] McAdams WH. Heat transmission. New York: McGraw-Hill; 1942.
[66] Fox W, Pritchard P, McDonald A. Introduction to fluid mechanics. New York: John Wiley & Sons; 2010 p. 754.